Please cite this article in press as: Xu et al., Interfaces in Solid-State Lithium Batteries, Joule (2018), https://doi.org/10.1016/j.joule.2018.07.009

Joule

CellPress
REVIEWS

Review

Interfaces in Solid-State Lithium Batteries

Lin Xu,[1,6] Shun Tang,[2,6] Yu Cheng,[1,6] Kangyan Wang,[3,6] Jiyuan Liang,[2] Cui Liu,[2] Yuan-Cheng Cao,[4,*] Feng Wei,[5] and Liqiang Mai[1,*]

The influence of interfaces represents a critical factor affecting the use of solid-state batteries (SSBs) in a wide range of practical industrial applications. However, our current understanding of this key issue remains somewhat limited. Therefore, this review presents the mechanisms and advanced characterization techniques associated with interfaces in SSBs. First, we compare liquid- and solid-state batteries and emphasize the challenges in solid-solid interfaces. Second, we discuss different aspects of interfaces including interphase formation, cathode-electrolyte interface, anode-electrolyte interface, and interparticle interface, which contain a detailed description of the formation mechanisms and current research. Third, the characterization strategies for effective interfacial observation and analysis are summarized and discussed. In particular, two unique characterization techniques, vibrational sum-frequency generation spectroscopy and on-chip single-nanowire battery characterization, are highlighted. Lastly, we summarize the scientific issues associated with solid-solid interfaces and provide our perspectives to better understand the fundamental issues and improve the performance of SSBs.

Introduction

As a key element in today's information-rich world and the devices that power it, rechargeable lithium-ion batteries (LIBs) are considered to be essential devices for a cleaner and more sustainable distributed energy supply.[1] However, safety issues and limited energy density are two of the major problems of current LIBs that feature organic liquid electrolytes. In contrast, the development of Li-air/Li anodes,[2–6] Li-S anodes,[2,4,7,8] and Si anodes[2,9,10] show promise for increasing energy density, providing that certain challenges can be overcome. For example, sharp, sticky Li dendrites that grow on the Li-metal anode during cycling, which can then penetrate through the separator between two electrodes, will induce sudden failure of the battery and the unwanted release of heat, the result of which is an increased fire hazard due to short-circuiting.[6,11] For an Li-S battery, in addition to safety concerns associated with dendrites, the polysulfides that form during cycling can dissolve into the liquid electrolytes, thus rendering the cell life too short for most applications without specified electrode modifications.[12–14] In addition, the insoluble Li_2S and/or Li_2S_2 products that cover the anode add extra internal resistance to the battery. With respect to an Si anode, the highest theoretical charge capacity of 4,200 mAh g^{-1}, which is due to multistep solid alloy reactions, is very impressive and has attracted a great deal of interest.[15] However, the huge volumetric change (~400%) upon lithiation and delithiation limits its application due to structural pulverization and a limited cycle life.[9] Considering both safety and performance, and the urgent challenges of meeting 21st-century power demands, the most promising direction for battery development is to use solid electrolytes, and preferably all solid-state batteries (SSBs).[3]

Context & Scale

Lithium-ion batteries (LIBs) are the promising power sources for portable electronics, electric vehicles, and smart grids. The recent LIBs with organic liquid electrolytes still suffer from safety issues and insufficient lifetime. Solid-state batteries (SSBs) are expected to address these issues. In principle, the nonflammable solid electrolytes could prevent battery combustion and explosion, and only Li ions are mobile in solid electrolytes, which could suppress side reactions. Some solid electrolytes, such as sulfides, have sufficiently high ionic conductivity, which is comparable to that of with organic liquid electrolytes. Thus, solid-solid interfaces appear to be the key to push SSBs toward practical applications. In this review, we start by introducing the challenges in solid-solid interfaces versus liquid-solid interfaces. We then discuss different interfaces in SSBs, including cathode-electrolyte interface, anode-electrolyte interface, and interparticle interface. Lastly, we present the advanced characterization techniques to help deepen understanding of the composition and structure evolution at the interfaces during battery cycling. The on-chip single-nanowire electrochemical devices developed by our group

Joule

CellPress
REVIEWS

A solid-state system yields many intriguing advantages.[16] First, a solid-state system alleviates safety concerns by abandoning the use of flammable organic liquid electrolytes. Second, it can potentially prevent short-circuits by blocking Li dendrites on one side. Third, some SSBs can be bent, punched, or even pierced without risking unwanted safety hazards. Fourth, the stable solid electrolyte potentially facilitates a wider electrochemical window, thereby enabling the use of certain cathode materials with higher voltage capability. It is worth noting that a recent study shows the electrochemical stability window of most inorganic solid electrolytes to be overestimated by the traditional Li/solid electrolyte/inert metal cell test (see detailed discussion in the subsection "Electrochemical Characterization").[17] All told, it is expected that SSBs will exhibit excellent cycle life, high reversibility, wider working temperatures, and other highly advantageous features. However, four specific standards must be met if the use of solid electrolytes is to be expanded: (1) high ionic conductivity, $\sigma_{Li^+} > 10^{-4}$ S cm^{-1}; (2) sufficient strength and minimum defects to inhibit Li dendrite penetration[18–20]; (3) affordable raw materials and facile fabrication methods; and (4) low activation energy for Li^+ diffusion.

In general, solid electrolytes can be divided into two major groups: organic solid polymers and inorganic solids, including oxides and sulfides, etc.[21] At present, a number of solid electrolytes with superb ionic conductivity have shown great promise to replace current commercial organic electrolyte batteries, especially for $Li_{10}GeP_2S_{12}$ and Li_2S-P_2S_5 with their high ionic conductivities of 1.2×10^{-2} S cm^{-1} and 1.7×10^{-2} S cm^{-1}, respectively. Their conductivity is comparable with that of organic liquid electrolyte (usually on the order of 10^{-2} S cm^{-1}, 25°C), indicating that solid electrolyte materials show great promise for next-generation batteries.[22,23] However, a key scientific issue that will hinder the practical application of SSBs concerns solid-solid interfaces.

In this review, we assess solid-state interfaces with respect to a range of important factors: interphase formation, interface between cathode and inorganic electrolyte, interface between anode and inorganic electrolyte, interface between polymer electrolyte and Li metal, and interface of interparticles. This review also summarizes existing characterization strategies, including microscopy observation, chemical composition analysis, and electrochemical characterization. Finally, we introduce several advanced methods that are used to comprehensively study interfaces in SSBs.

Challenges in Solid-Solid Interfaces versus Liquid-Solid Interfaces

For a liquid-electrolyte system, wetting enables the liquid electrolyte to be fully infiltrated in the electrode, thereby facilitating simultaneous Li^+ intercalation/conversion/alloying reactions for all active materials in the electrode, assuming that the time gap for electron transport can be overcome. Charge carriers in the electrolyte reduce with the consumption of Li^+ during solid-electrolyte interphase (SEI) formation, further increasing the resistance for ion transfer and therefore hindering the ability for high-rate charging/discharging. Although electrolyte decomposition can be partially recovered through the use of a stable SEI and additional electrolytes in the battery wetting the electrode, this phenomenon is less obvious for anodes such as $Li_4Ti_5O_{12}$ (LTO, ca. 1.5 V versus Li^+/Li), Li-In alloy (0.6 V versus Li^+/Li), and others.[24]

Briefly there are four key challenges in SSBs versus liquid batteries. First, the ionic conductivity of most solid-state electrolytes is lower than that of liquid electrolytes. Although some sulfide electrolytes can achieve high ionic conductivity, a number

are highlighted as a unique platform for *in situ* characterization.

We suggest and emphasize some future directions for SSBs. First, different *in situ* or *operando* characterization techniques should be developed and combined to track the real-time composition and structure changes at the interfaces in SSBs. Second, in addition to metal ions, metal-air and metal-sulfur systems with much higher energy density should also receive sufficient attention for SSBs. Lastly, a unique advantage of SSBs over liquid-electrolyte batteries is that SSBs could be flexible, stretchable, and shrunk on a chip. Thus, SSBs are promising for integration with microelectronic circuits to fabricate self-powered wearable or implantable micro-/nanoscale devices.

[1]State Key Laboratory of Advanced Technology for Materials Synthesis and Processing, International School of Materials Science and Engineering, Wuhan University of Technology, Wuhan 430070, China

[2]Key Laboratory of Optoelectronic Chemical Materials and Devices, Ministry of Education, School of Chemical and Environmental Engineering, Jianghan University, Wuhan 430056, China

[3]Department of Chemical Engineering, University of Melbourne, Melbourne, VIC 3010, Australia

[4]State Key Laboratory of Advanced Electromagnetic Engineering and Technology, School of Electrical and Electronic Engineering, Huazhong University of Science and Technology, Wuhan 430074, China

[5]Institute for Interdisciplinary Research, Jianghan University, Wuhan 430056, China

[6]These authors contributed equally

*Correspondence: caosome@126.com (Y.-C.C.), mlq518@whut.edu.cn (L.M.)

https://doi.org/10.1016/j.joule.2018.07.009

Please cite this article in press as: Xu et al., Interfaces in Solid-State Lithium Batteries, Joule (2018), https://doi.org/10.1016/j.joule.2018.07.009

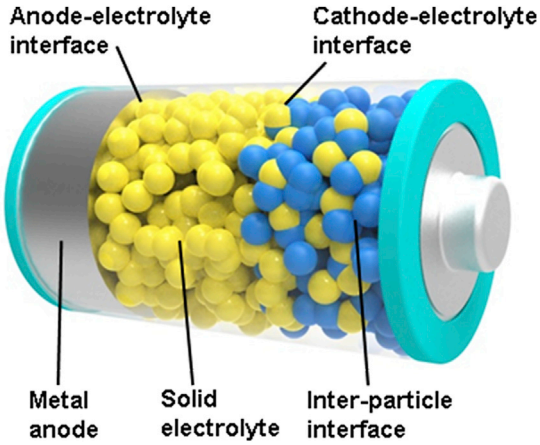

Figure 1. Schematic of Different Interfaces in Solid-State Batteries

For the purpose of highlighting the interfaces, the size of particles and grain boundaries in this schematic are not proportional. The schematic only presents the general structures of inorganic solid-electrolyte batteries, and some specific components—notably conductive additives and polymer electrolytes in other batteries—are not shown.

of instability issues at the interface must be addressed. Second, in contrast to liquid electrolytes, the interfacial compatibility between solid electrolytes and electrodes is usually poor and needs significant improvement for application in SSBs. The interfaces in an inorganic solid-electrolyte battery can feature several basic structures: the cathode-electrolyte interface, the anode-electrolyte interface, and the interparticle interface, as illustrated in Figure 1. In addition to the ionic conductivity of the electrolyte, ionic transport of Li^+ at the interfaces also determines the overall ionic conductance that ultimately defines the rate performance of these batteries. This relationship explains why overall electrochemical impedance can be high, even in cases when the ionic conductivity of a solid electrolyte is excellent, as well as why achieving high Li^+ conductance in the solid state comparable with existing liquid electrolytes is a challenging task. In industrial settings, for example, the best electrolyte-electrode interaction is achieved by enabling the wetting of the electrodes with electrolytes for a week or even two (and even in a laboratory setting, a day's wetting is required). Adopting a solid bulk that has literally no self-diffusion—in other words, a "wetting effect"—can lead to severe interface impedance. In addition to the conventionally conceived electrolyte-electrode interface, an electrode's interparticle interface also plays a prominent role in a composite electrode material. For example, the relatively low electronic and ionic conductivities of cathodes that occur as a result of poor contact at the phase-phase or particle-particle interface could limit efforts to improve the power density of SSBs.[25] Third, preventing Li dendrite penetration is still challenging in SSBs, even for ceramic electrolytes with high mechanical strength. Fourth, despite growing research efforts to elucidate the formation of interphases between solid electrolytes and electrodes, we still do not have a complete understanding of the microstructure, dynamic behavior, and chemical reactivity of SEI during cycling. Thus, advanced characterization techniques that provide *in situ* and real-time information about batteries in a working environment are essential for the further development of SSBs.

Interfaces in Solid-State Batteries

We define the term "interface" as a combination of interphase formation, contact condition, energy status, and defects. Physical and chemical processes that take place at an interface during cycling should be taken into consideration. These essential processes include SEI formation, dendrite growth, Li-depleted space-charge layer, and interfacial adhesion variation due to structural and volume change, among

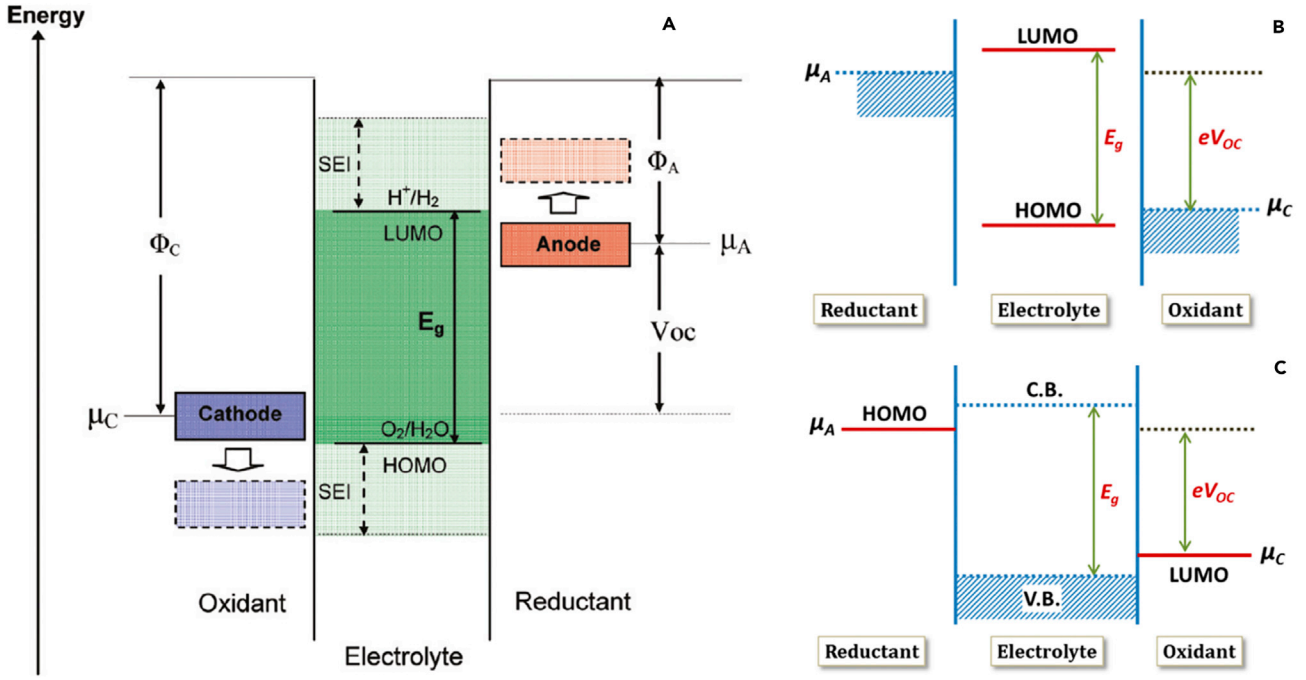

Figure 2. Open-Circuit Energy Diagrams of Different Battery Systems

(A) Overall illustration of a battery with a liquid electrolyte. μ_a and μ_c refer to energy levels of anode and cathode materials, respectively. LUMO and HOMO represent the lowest unoccupied molecular orbital and highest occupied molecular orbital of liquid electrolyte, respectively. C.B. refers to the conducting band of solid electrolyte and V.B. indicates the valance band. V_{oc} refers to the open-circuit voltage of the battery. Reprinted from Goodenough and Kim,[26] with permission. Copyright 2009, American Chemical Society.

(B) Stable energy window for liquid electrolyte.

(C) Stable energy window for solid electrolyte.

(B) and (C) are reprinted from Goodenough and Park,[1] with permission. Copyright 2013, American Chemical Society.

others. This section features a detailed discussion of interphase formation and different categories of interfaces and their particular characteristics.

Interphase Formation

Understanding the interfacial reaction is important, as it provides critical information on the interfacial products (interphase) and their various effects on the stability and electronic performance of a SSB. The chemical stability of an electrolyte can be predicted using the energy diagram shown in Figure 2. The "window" for both liquid and solid electrolytes can be determined by the energy separation E_g between the lowest unoccupied molecular orbital (LUMO) or conducting band (CB) and the highest occupied molecular orbital (HOMO) or valence band (VB)[1,26] of the electrolyte material, which is thermodynamically stable when the chemical potential (μ_a for anode and μ_c for cathode) of the electrode materials is within the LUMO-HOMO range. In other words, the interface is not stable if μ_a > LUMO (or CB) or μ_c < HOMO (or VB), unless an SEI forms at the interface as the passivation layer. The formation of SEI has been widely studied in liquid-electrolyte batteries, and the concept can potentially be extended to SSBs upon careful comparison of these two very different battery systems.[27–29]

The interfacial reaction and the interphase products play important roles in reaching the full potential of SSBs, as Li^+ ions diffuse from the bulk electrolyte mostly via Schottky vacancy and grain boundaries.[30,31] The structure, contact condition,[32] and even the electronegativity[33] of the interphase all affect the resulting energy

delivery of SSBs. Zhu et al. carried out theoretical predictions of the reduction/oxidation potential and the phase equilibria of many conventional solid electrolytes.[34,35] Importantly, their theoretical results agree with a series of recent experiments. For example, X-ray diffraction (XRD) was used to characterize Li_2S at the Li/LGPS interface (LGPS stands for $Li_{10}GeP_2S_{12}$) and unknown products at the acetylene black/LGPS interface.[36] Additional studies have characterized Li_3P, Li_2S, and $Li_{15}Ge_4$ at the Li/LGPS interface, as well as the reduction product of $Li_{3x}La_{2/3-x}TiO_3$ (LLTO) and $Li_{1+x}Al_xTi_{2-x}(PO_4)_3$ (LATP).[37,38] Furthermore, *in situ* X-ray photoelectron spectroscopy (XPS) has been utilized to characterize Li_3N, Li_2O, and Li_3P at the Li/LiPON (lithium phosphorous oxynitride) interface.[39] Quite recently, XPS was also used to confirm that the once-believed extremely stable $Li_7La_3Zr_2O_{12}$ (LLZO) was reactive with Li at 300°C–350°C.[40] Additional studies conducted by Wenzel et al. using *in situ* XPS determined that (1) the decomposed $Li_{10}GeP_2S_{12}$ interphase consists of Li_3P, Li_2S, and Li-Ge alloy,[37] and (2) decomposed LLTO interphase consists of Ti^{3+}, Ti^{2+}, and Ti metal.[41] A detailed discussion of several characterization techniques is included in the section "Advanced Characterization Techniques". It is worth noting that some sulfide materials have been found to exhibit both excellent Li^+ ion conductivity and electrochemical stability—principally $Li_{9.54}Si_{1.74}P_{1.44}S_{11.77}Cl_{0.3}$[32,42] and $Li_{9.6}P_3S_{12}$.[42] A further understanding of the nature and behavior of interphase materials, including their formation mechanisms, conductivity for electrons/ions, mechanical strength, and crystal structure is absolutely essential for advancing the science of battery chemistry.

Interface between Cathode and Inorganic Electrolyte

Unlike metal anodes, cathode materials are composed of particles of active materials such as $LiCoO_2$ (LCO), $LiMn_2O_4$ (LMO), $LiNiMnCoO_2$, $LiNiCoAlO_2$, and $LiFePO_4$ that are mixed with appropriate amounts of solid electrolytes (ionic conductors), carbon (electronic conductors) and/or binders to enhance the ionic and electronic transport. In liquid-electrolyte batteries, the liquid electrolyte wets the gaps between the cathode particles as well as the gaps between the electrode and electrolyte; in contrast, physical contact is expected for solid-solid interfaces in SSBs. To clarify the effects of each interface, Luntz et al.[43] employed a symmetric cell to evaluate the internal resistance (IR) drop at the cathode-electrolyte interface and anode-electrolyte interface. Their assessment scheme and results are shown in Figures 3A–3D. In their experiment, an Au/SSE/Au cell (SSE refers to solid-state electrolyte) served as the baseline for their IR drop measurements. The SSE featured LiPON with low reduction voltage and Li^+ conductivity at a magnitude of 10^{-5}–10^{-6} S cm^{-1}. For the Li/SSE/Li cell, a slight IR drop was evidenced, confirming an interface resistance between Li and SSE. However, when they combined SSE with carbon cathodes (Figures 3C and 3D), the IR drop increased much more significantly in comparison with analogous results for Li, indicating a much higher interfacial resistance. The IR drop on the Li/SSE interface could be attributed to the formation of SEI and an incomplete contact; for the cathode-electrolyte interface, however, the electrochemical processes can be much more complicated. Although their results do shed light on the different contributions of interface resistance at the cathode and anode, they only considered carbon cathodes in reporting that the highest interface resistance occurs at the cathode-electrolyte interface.

Several kinds of interfacial resistance can coexist at the same time. One type of resistance is contact resistance, which results from poor interfacial contact or contact loss during cycling[44,45]; thus, secure contact will reduce interfacial resistance. For instance, Ohta et al.[44] assembled a LCO/$Li_{6.75}La_3Zr_{1.75}Nb_{0.25}O_{12}$/Li SSB with ultrafine LCO/LLZO interfacial contact (Figures 3E–3G). This battery exhibits excellent

Joule

CellPress REVIEWS

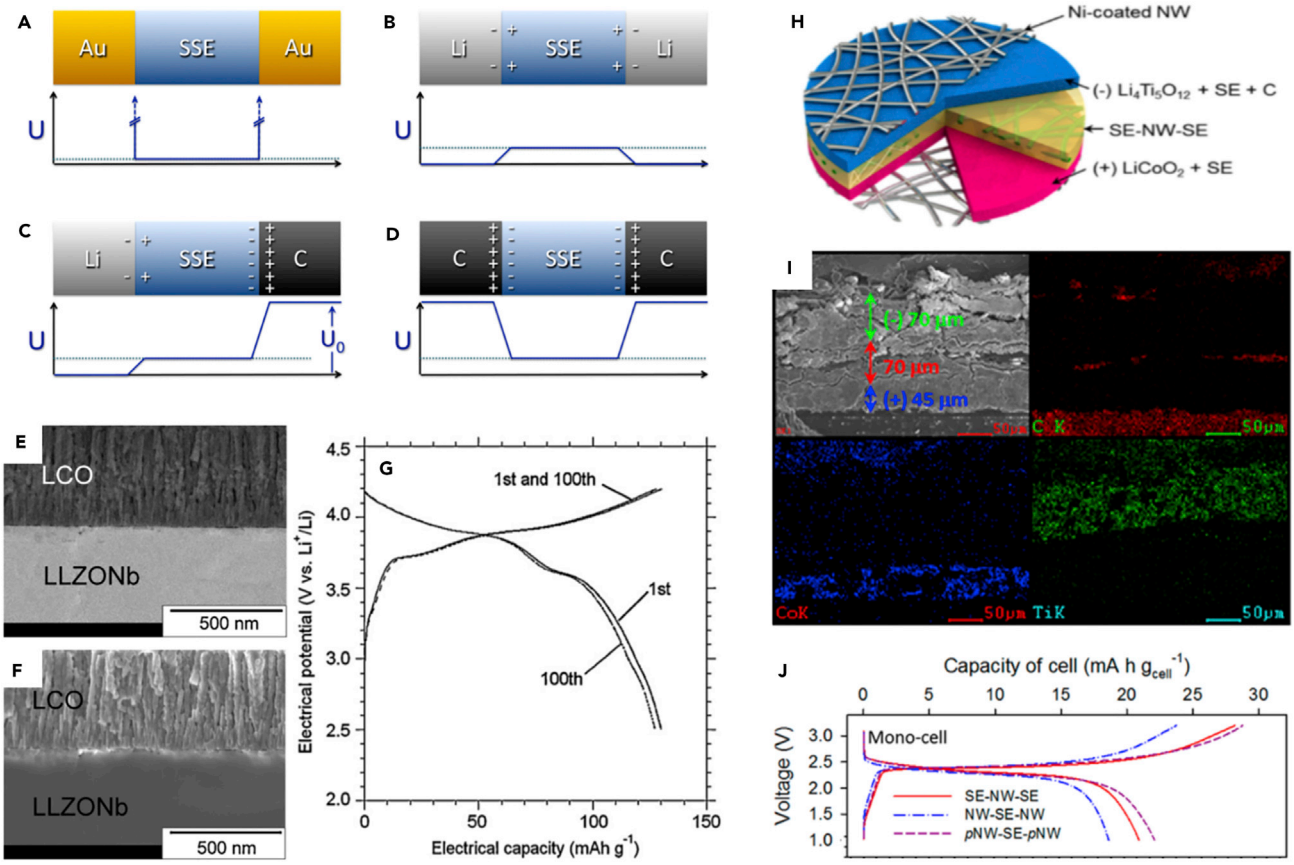

Figure 3. Typical Examples of Cathode-Electrolyte Interfaces in Solid-State Batteries

(A–D) Various symmetric cell models and potential profiles. Note that SSE refers to solid-state electrolytes. Au|SSE|Au symmetric cell (A). Li|SSE|Li symmetric cell (B). Li|SSE|C asymmetric cell (C). C|SSE|C symmetric cell (D). Reprinted from Luntz et al.,[43] with permission. Copyright 2015, American Chemical Society.

(E–G) Cross-section scanning EM image (E), backscattering electron image after 100 cycles (F), and charge/discharge curves in first and 100th cycles (G) of the LCO/LLZO/Li battery, respectively. Reprinted from Ohta et al.,[44] with permission. Copyright 2012, Elsevier B.V.

(H–J) Schematic of the battery configuration (H), cross-section scanning EM image and EDS mapping (I), and charge-discharge curves (J) of flexible SSBs. Reprinted from Nam et al.,[45] with permission. Copyright 2015, American Chemical Society.

cycling reversibility. Han et al.[46] modified the interface between LCO and LLZO by thermally soldering them together with $Li_{2.3-x}C_{0.7+x}B_{0.3-x}O_3$ SEI, which effectively decreased the interfacial resistance and achieved high cycling stability. Additionally, Nam et al.[45] assembled flexible SSBs by utilizing polymer scaffolding (Figures 3H–3J), whereby an interfacial contact was maintained. There is another type of resistance that results from the nanoionic effect, which is a space-charge layer generated at the interface between two ionic conductors with different chemical potentials of the ions. In brief, a sulfide solid electrolyte has lower chemical potential of Li^+ and weaker attraction to Li^+ compared with a high-voltage cathode, such as $LiCoO_2$. When a sulfide solid electrolyte comes into contact with $LiCoO_2$, Li^+ will diffuse from the electrolyte side to the cathode side, generating a high-resistance Li depletion layer at the interface on the electrolyte side (Figures 4A and 4C).[33,47] Such a space-charge zone is detrimental and severely affects the high-rate charge/discharge ability of SSBs, while also serving as the rate-determining step.[48–50] Suppression of this effect is essential for producing high-power density SSBs. One possible way to inhibit the nanoionic effect is to shield the sulfide with a thin oxide buffer layer that prevents direct contact with the cathode (Figures 4B and 4D). For example, coating $LiNbO_3$ on LCO[50] and LMO[51] could successfully suppress the

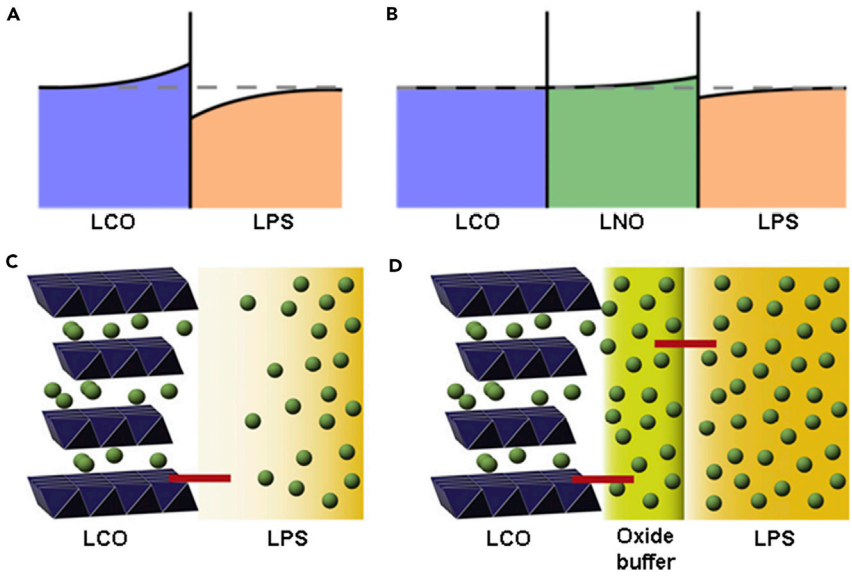

Figure 4. Illustration of Nanoionics Effect in Sulfide Electrolyte Interface

(A and B) Lithium concentration profiles at the LCO-LPS interface without (A) and with (B) an LNO buffer layer. The dashed lines represent lithium chemical potential as the reference. Here LCO, LPS, and LNO refer to $LiCoO_2$, Li_3PS_4, and $LiNbO_3$, respectively. Reprinted from Haruyama et al.,[47] with permission. Copyright 2014, American Chemical Society.

(C and D) Space-charge zone in LCO-sulfide electrolyte interface without (C) and with (D) buffer. Reprinted from Takada,[33] with permission. Copyright 2013, Elsevier B.V.

space-charge layer effect. In many cases, capacity fading is caused by simultaneous negative effects. Koerver et al. discovered that at the interface of $LiNi_{0.8}Co_{0.1}Mn_{0.1}O_2$ and β-Li_3PS_4, capacity fading stems from the decomposition of sulfide electrolytes and volume shrinking of cathode materials, which results in contact loss.[52]

It has been widely observed that intercalation reaction electrodes exhibit better cycling reversibility than alloy and conversion reactions in LIBs. The structure stability is even more important in solid-state systems. Thus, a complex framework such as carbon coating is required, especially for alloy or conversion reactions involving a sulfur cathode. However, at the interface between the cathode and sulfide electrolyte, the carbon additives that provide electronic percolation paths accelerate the interfacial oxidation reaction. The formed polysulfide by-products block Li^+ conduction paths, leading to significant interfacial resistance and irreversible capacity loss.[53] Hence, the compatibility between electrolytes and electrodes should be carefully considered when designing the composition and structure of electrode materials.

Interface between Anode and Inorganic Electrolyte

In this section only a Li anode will be discussed, although it must be noted that this analysis is also applicable to Si anodes and carbon anodes. We begin this discussion by examining Li nucleation and growth in liquid electrolytes to better understand the fundamental issues involved in this process, and then extend this analysis to include Li penetration through solid electrolytes. A long-standing problem for Li anodes is associated with dendrite growth that penetrates the electrolyte and causes short-circuiting,[31,54] which also contributes to the intrinsic high activation energy.[55] The nucleation and growth of Li on Li metal upon cycling occurs quite rapidly. SEI on

Li cannot provide sufficient mechanical strength to prevent dendrite formation if penetrated. Thus, atomic force microscopy (AFM) represents a powerful tool to monitor the surface topography and modulus of the interface, while *in situ* AFM studies have been conducted to show that the Young's modulus of natural SEI layer in organic electrolyte is within the range of 50–400 MPa.[56,57] The result is that the Li surface may become bumpy, resulting in undesirable interfacial contact. Various Li growth mechanisms have been assessed in prior reviews.[6,30]

The Cui group studied the effects of overpotential on Li nucleation and growth at the nanoscale level, which include several key results.[58] First, the Li nucleation energy barrier increases with overpotential (Figure 5A). Second, during galvanostatic Li deposition, the potential initially drops to $-\eta_n$ (η_n refers to nucleation overpotential) to initiate the nucleation, then rises to $-\eta_p$ (η_p refers to plateau overpotential) for steady-state Li growth (Figure 5B). Third, an inverse relationship exists between the size of Li nuclei and overpotential; additionally, there is a cubic relationship between the density of Li nuclei and overpotential (Figure 5C). Fourth, experimental data indicate that the nucleation barrier and growth plateau increase with galvanostatic current density (Figure 5D). Overall, these results suggest that small, dense, and uniform Li nuclei can grow when the overpotential is increased via high current density. This fundamental study on Li nucleation and growth can rationally guide the design of micro-/nanostructures for Li-metal anodes and the optimization of charge/discharge conditions.

Compared with liquid electrolytes, different issues must be considered in the case of solid electrolytes. Recently, Porz et al. reported the process of Li dendrite growth and infiltration in inorganic solid electrolytes.[31] For their study, they selected different inorganic solid electrolytes including sulfide and garnet electrolytes. Their results confirmed that Li penetration depends on defect size and density rather than on the impact of electrolyte shear modulus and surface roughness. Moreover, the researchers showed that the flaws/cracks, grain boundaries, and/or micro-/nanoscale pores usually lead to faster Li dendrite growth and crack propagation. Accordingly, they developed a model and studied the dependence of Li deposition overpotential and the stress-crack propagation relationship on defect size for $Li_6La_3ZrTaO_{12}$ and glassy Li_2S-P_2S_5 (Figure 5E). Both the minimum overpotential and crack-extension stress decreased with defect size with inverse square-root dependence. Thus, strategies for minimizing interfacial defects represent a critical design principle for inhibiting Li dendrite penetration in inorganic solid electrolytes.

Interface between Polymer Electrolyte and Lithium Metal

Although current polymer electrolytes cannot compete with ceramic or glass electrolytes in terms of ionic conductivity, the versatility of polymer electrolytes is still highly desirable in the development of flexible batteries and electronics.[59,60] The advantage of using a liquid electrolyte is that the flowability of liquid ensures the maximum electrolyte-electrode contact area and minimum electronic resistance.[32] These desirable attributes can be inherited by polymer electrolyte that also features good adhesiveness and malleability. In addition to low conductivity, another issue for a polymer electrolyte is Li dendrite formation. Utilizing Mullins-Sekerka linear stability analysis and the Barton and Bockrisis dendrite-propagation model, Monroe and Newman concluded that (1) dendrite growth at all applied current values, and (2) morphological instability are both essentially insurmountable for a Li-polymer interface once the system has reached the propagation regime.[20,54] However, they predicted that interfacial stability can be achieved when the shear modulus of the polymer is in the gigapascal (GPa) range.

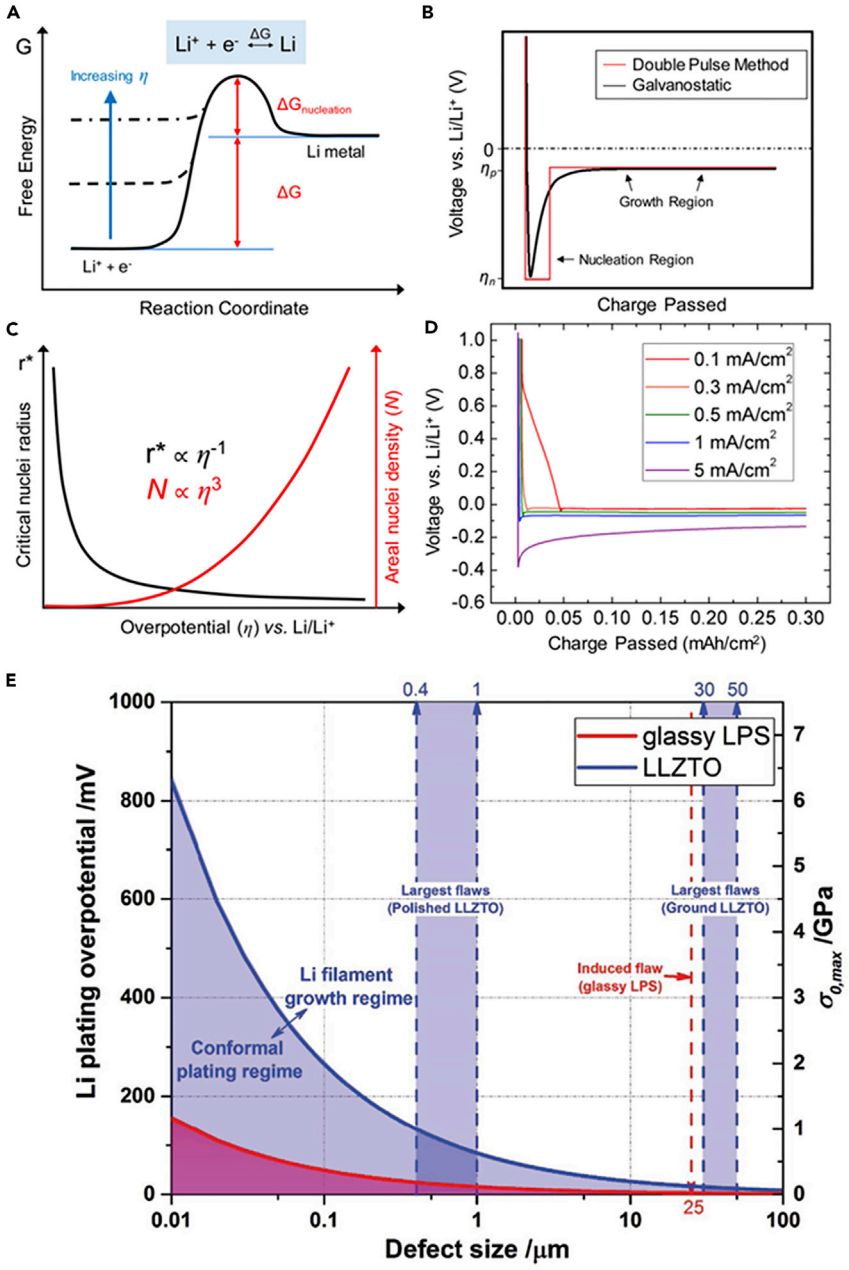

Figure 5. Lithium Nucleation, Growth, and Penetration

(A) Schematic relation of overpotential and Li nucleation energy barrier.

(B) Schematic voltage profiles of Li deposition with galvanostatic and double-pulse method.

(C) Schematic plots of the size and density of Li nuclei versus overpotential.

(D) Experimental voltage profiles of Li deposition at different current densities.

(E) Diagram of the relation of Li plating overpotential, crack-extension stress, and defect size. Here, LPS and LLZTO refer to Li_2S-P_2S_5 and $Li_6La_3ZrTaO_{12}$, respectively. Reprinted from Porz et al.,[31] with permission. Copyright 2017, Wiley-VCH.

(A)–(D) are reprinted from Pei et al.,[58] with permission. Copyright 2017, American Chemical Society.

For years, one of the primary challenges in utilizing polymer electrolytes had been increasing mechanical properties without sacrificing ionic conductivity. Mechanical strength can be enhanced through a variety of approaches, including increasing

molecular weight, adding substitute groups, crosslinking, copolymerization, and enhancing crystallinity. Meanwhile, ionic conductivity can be simply enhanced by adding and optimizing salt component.[61] However, there are other methods for achieving both high ionic conductivity and mechanical strength. For instance, Schulze et al. applied a polymerization-induced phase separation method where ion-conducting domains and high-modulus domains are mixed in one system, thereby achieving 1 GPa elastic modulus and 1 mS cm^{-1} ionic conductivity at the same time.[62] Note that the Newman model is only applicable for polymers and not inorganic solid-state electrolytes, because the defects and grain boundaries significantly affect the penetration of Li dendrites through inorganic solid-state electrolytes.

In addition to Li dendrite penetration, chemical stability and Li-polymer adhesion should also be considered when designing polymer electrolyte batteries. One important application for a Li anode is in Li-air batteries. During battery discharge, oxygen will first reduce to superoxide radical anions and then form LiO_2 and Li_2O_2 consecutively. Meanwhile many aprotic electrolytes are not stable against these two products, which has the unwanted outcome of shortening the cycle life of the batteries. Amanchukwu et al. analyzed nine types of polymers and discovered that only three were chemically stable.[63] Thus, understanding the reactivity of polymers and reaction products provides critical information for the design of polymer electrolytes for use in next-generation batteries and devices. In terms of Li-polymer adhesion, this facet is not well understood because conventional models view the electrolyte-electrode interface as simply a boundary condition.[20,54] Dendrite penetration in polymers is unlike what occurs with solid-state oxides or sulfides where Li grows through the grain boundaries and defects. Therefore a shear modulus in the range of GPa is needed to suppress dendrite formation, as Monroe and Newman predicted.[20,54] Moreover, Li anodes are known to recede a few microns during discharge if the polymer does not have a good adhesion to the Li; thus, the resulting void will eventually increase interfacial resistance and decrease overall ionic conductivity.[64] In short, excellent adhesion between a Li metal and the selected polymer is essential to ensure efficient ion transfer and long cycle life.

Interface of Interparticles

In general, ionically and/or electrically conductive particles must be added and mixed with the active material particles during the fabrication process of a cathode or anode of a SSB if the active materials are not highly ionically and/or electrically conductive. Thus, the interparticle interface in a composite cathode or anode is also important. The definition of this interface includes both the interface between active materials and the contact between active material particles and ionically/electrically conductive particles. Lithium ions transport through the electrodes via grain boundaries. The volume change of the cathode particles during charge/discharge would lead to contact failure in composite electrodes.[65]

Strauss et al. studied the effect of the size of cathode composite materials, reporting that cathode materials of a smaller particle size (much less than 10 μm) will deliver near-full capacity in the first cycle, which is due to both increased electrical contact as well as the fact that there are more consecutive grain boundaries—meaning that ions will transport with less resistance.[66] They pointed out that the ratio of solid-electrolyte particles to cathode particles in a given composite cathode should be determined according to the desired purpose.[66] For example, a high-energy-density battery requires fewer solid-electrolyte particles; in contrast, a high-power-density battery requires more solid-electrolyte particles in the composite cathode. It is worth

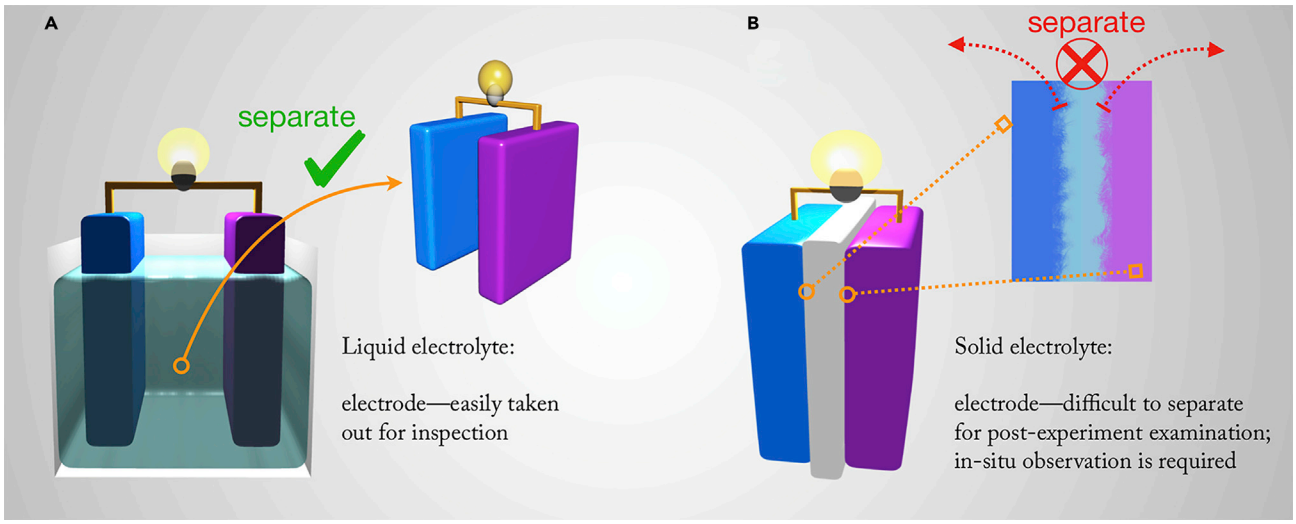

Figure 6. Schematics of Typical Interfacial Contact in a Liquid Electrolyte Battery and a Solid Electrolyte battery
Illustration of the difficulty of investigating a liquid-electrolyte battery (A) and a solid-electrolyte battery (B).

noting that there should be a balance of ionic and electronic paths within a composite electrode. On the one hand, the presence of too many electrolyte particles blocks the electronic path. On the other hand, too many active cathode particles will limit ionic transport. Rational micro-/nanostructure designs—for example, adopting hierarchically mixed ion- and electron-conducting networks—could facilitate ionic transport while reducing electronic resistance.

Advanced Characterization Techniques

The type and behavior of an interface in a SSB represent key issues due to the degree of contact and high charge transfer impedance at the interface.[67–69] Therefore, it is essential to clarify the interfacial impedance phenomena as evidenced by morphological changes and electrochemical processes via the use of advanced characterization techniques. Only then can next-generation SSBs that meet a wide range of industrial and personal consumer demands be developed. Although various methods have been established to investigate liquid-electrolyte battery systems, a formidable obstacle remains in determining interfacial behavior in SSBs. Indeed, such interfaces are difficult to isolate compared with their counterparts in liquid-electrolyte systems. As can be seen in Figure 6, electrode materials in liquid-electrolyte systems are rather easy to extract for post-experimental analysis without damaging the sample materials. In contrast, to fabricate a SSB various methods such as hot-pressing technology and chemical/physical evaporation are usually carried out to obtain a relatively superior interfacial contact.[70] Thus, these tightly embedded interfaces cannot be fully exposed without damaging the surface condition, making it difficult to obtain essential information about their interfacial reactions and kinetics, especially in the case of Li anode/solid-electrolyte systems.[41] Hence a different approach, ideally involving an *in situ* experimental methodology, must be designed.[71] Typically electrode materials are studied by *ex situ* experiments in coin cells, but interfacial studies could be carried out by hybrid cell,[70] symmetric cell,[43] or through a combination of *ex situ* and/or *in situ* experiments. As evidenced in the energy diagram (Figure 2), two kinds of interfaces can be distinguished: thermodynamic stable interface and thermodynamic unstable interface (representing the majority at present). In this section, the currently available interfacial

characterization methods are organized into three categories. In addition, two advantageous characterization methods developed by our collaborative group are highlighted.

Microscopy Observation

Unlike conventional microscopic investigations of liquid-electrolyte batteries, the intact interfaces in SSBs are difficult to isolate for microscopy characterization. A cross-section image of the anode-electrolyte interface or cathode-electrolyte interface provides more convincing results, but specific techniques for sample preparation are required. If a more effective way, such as focus ion beam, could be developed to cut the cross-section of the sample with precision, many conventional methods such as cross-section scanning electron microscopy (EM) (Figures 7I and 7P show the clear cross-section scanning EM images of the interface between electrode and electrolyte,[72] transmission electron microscopy (TEM), energy-dispersed X-ray analysis (EDX), and electron energy loss spectroscopy (EELS) could be utilized to elucidate the nature of the interface. Moreover, by switching different modes of TEM (image, diffraction, and spectroscopy) and combining results with those obtained using EDX[73] and EELS, more detailed information about morphology, structure, and composition of the Li_2SiO_3-coated $LiCoO_2$/Li_2S-P_2S_5 interface could also be accurately obtained (Figure 7E).

As shown in Figure 7, there are numerous successful microscopic observations. These photos include one or two kinds of interfaces in one frame. The difficulty in obtaining two kinds of interfaces in one frame is related to microbattery sample preparation. Special sample holders are essential to prevent air exposure. Brazier et al.[77] used pulsed laser deposition (PLD) to prepare a microcell and was the first to perform direct *in situ* TEM observations. Later, cross-section images of the interface between $LiCoO_2$ and Li_2S-P_2S_5 were obtained by high-angle annular dark-field scanning TEM (HAADF-STEM) (Figures 7A–7D and 7M–7O)[74]; this study, in particular, opened up the door for interfacial TEM observations and later *in situ* experiments. The charge-discharge reaction process of a Li-oxygen battery was observed in real time by the *operando* liquid cell EM. The reaction details for Li ions and oxygen at the interface between the carbon cathode and the liquid electrolyte could be observed at the nanometer and millisecond levels.[78] Santhanagopalan et al. improved upon their previous *ex situ* scanning TEM (STEM)-EELS[79] technique, and introduced an *in situ* STEM-EELS (Figures 7F–7H)[75] interfacial approach. Subnanometer resolution, subsecond temporal resolution, and even atomic percentage light element detection can be achieved with this state-of-the-art STEM-EELS technique.[75,76,79,80] Furthermore, Li_3N, Li_2CO_3, and LiO_x were found along the grain boundaries of HP-LLZ:Ta (hot-pressed Ta-substituted $Li_7La_3Zr_2O_{12}$) (Figures 7J–7L) by high-resolution TEM (HRTEM)-EELS.[76] AFM is another popular method for obtaining surface characterization information.[31,56,57] Recently, Shen et al. utilized *in situ* electrochemical AFM to investigate Li dendrite growth on graphite anodes[81] using different liquid electrolytes. This approach has not yet been applied to solid systems, but we are optimistic that this possibility will eventually become a reality. Other methods such as Auger electron spectroscopy, time-of-flight secondary ion mass spectroscopy, and scanning tunneling microscopy can also be implemented with *ex situ* experiments or designed for *in situ* investigations.

Chemical Composition Analysis

The instability of an interface often stems from the degradation of electrolytes, which is an important factor affecting the performance of SSBs. The Ceder group has obtained a large number of calculations with DFT[82] and first principles[83] on the

interfacial stability between the electrode and the solid electrolyte. In particular, they studied the thermodynamics of interfacial phases and found that generally, electrolytes that are stable at the cathode voltage show low reaction energies. They calculated that thiophosphate electrolytes have especially high reactivity with high-voltage cathodes (such as LCO) and a narrow electrochemical stability window. They also proposed a number of intriguing battery combinations with high energy that had not been employed, such as Li_3PS_4 or $Li_7P_3S_{11}$ combined with $LiVS_2$, $LiTiS_2$ cathode with Li_2S-P_2S_5, and $LiBH_4$-$LiTiS_2$ cells.[84] Most recently, they reported that Li demonstrates the highest stability at the tetrahedral site and that the body-centered cubic-like anion framework is the most desirable for achieving high ionic conductivity.[16] These novel and significant design advances serve as a good guide for the development of fast ion-conducting materials.

Chemical composition investigations are mainly utilized to verify the chemical stability of the electrolyte-electrode interface, which can share the same purpose as cyclic voltammetry (CV) but with higher accuracy since it can be measured quantitatively. XPS and Fourier transform infrared spectroscopy are the most widely used techniques for SEI investigations.[27] For organic liquid-electrolyte batteries, coin cells are dissembled in a glovebox and samples are washed with an organic solvent before undergoing examination. While these techniques can be employed if SSBs have similar circumstances, for most cases a cross-section cut is needed. XRD has long been utilized as a standard method to assess composition analysis,[36] and single-crystal XRD remains the most effective and convincing way to determine the anisotropic displacement parameter of a new material.[85] Crystals can be regarded as diffraction gratings for X-rays, and the coherent scattering produced by a large number of these particles will interfere with the light, thereby increasing or decreasing the intensity of scattered X-rays. Therefore, the crystal phase composition and unit cell parameters can be detected by XRD, and different peak positions are caused by different crystal structures. In contrast, amorphous materials do not have a complete crystal structure and are difficult to detect by XRD. Unlike XRD, XPS works on the chemical bond, and X-rays can interact with atoms in the material's surface layer to produce photon energy. When the photon energy generated exceeds the binding energy in the electronic nucleus, it will stimulate the inner layer of electrons in the atom, thereby producing photoelectrons. Detecting the quantity and kinetic energy of photoelectrons through the corresponding testing instruments enables XPS technology to accurately analyze the content and chemical state of the elements in the sample surface. Zhang et al. coated LLTO with Li_2O-B_2O_3, and resulting XRD characterization results showed no added peaks compared with the pure LLTO. The researchers then speculated that Li_2O-B_2O_3 was present in the grain boundary of LLTO, which was later confirmed by XPS.[86] Although Demir-Cakan et al. detected the deposition of Li_2S on a Li anode via XRD, they also conducted XPS characterization to clearly verify the surface decomposition.[87] Hence, XPS is a vital tool in interface detection.

Dedryvère and colleagues studied SEI formation[87,88] and the Li-ion transfer mechanism[89] between the electrode and liquid-electrolyte interface by *ex situ* XPS. They observed that in the silicon anode SEI initially forms on the anode, after which Li and silicon formed an alloy to achieve the lithiation process, with the generation of Li_2O and Li_xSiO_4. After full charging, the thickness of the SEI decreased only slightly and the Li_2O disappeared.[89] In the case of electrolytes they reported that $EC_{0.45}$:$PC_{0.45}$:$DMC_{0.1}$ (EC, PC, and DMC refer to polycarbonate, ethylene carbonate, and dimethyl carbonate, respectively) with 1 M of Na salt was an optimal electrolyte formulation that could effectively suppress the degradation of the electrolyte

Joule

CellPress
REVIEWS

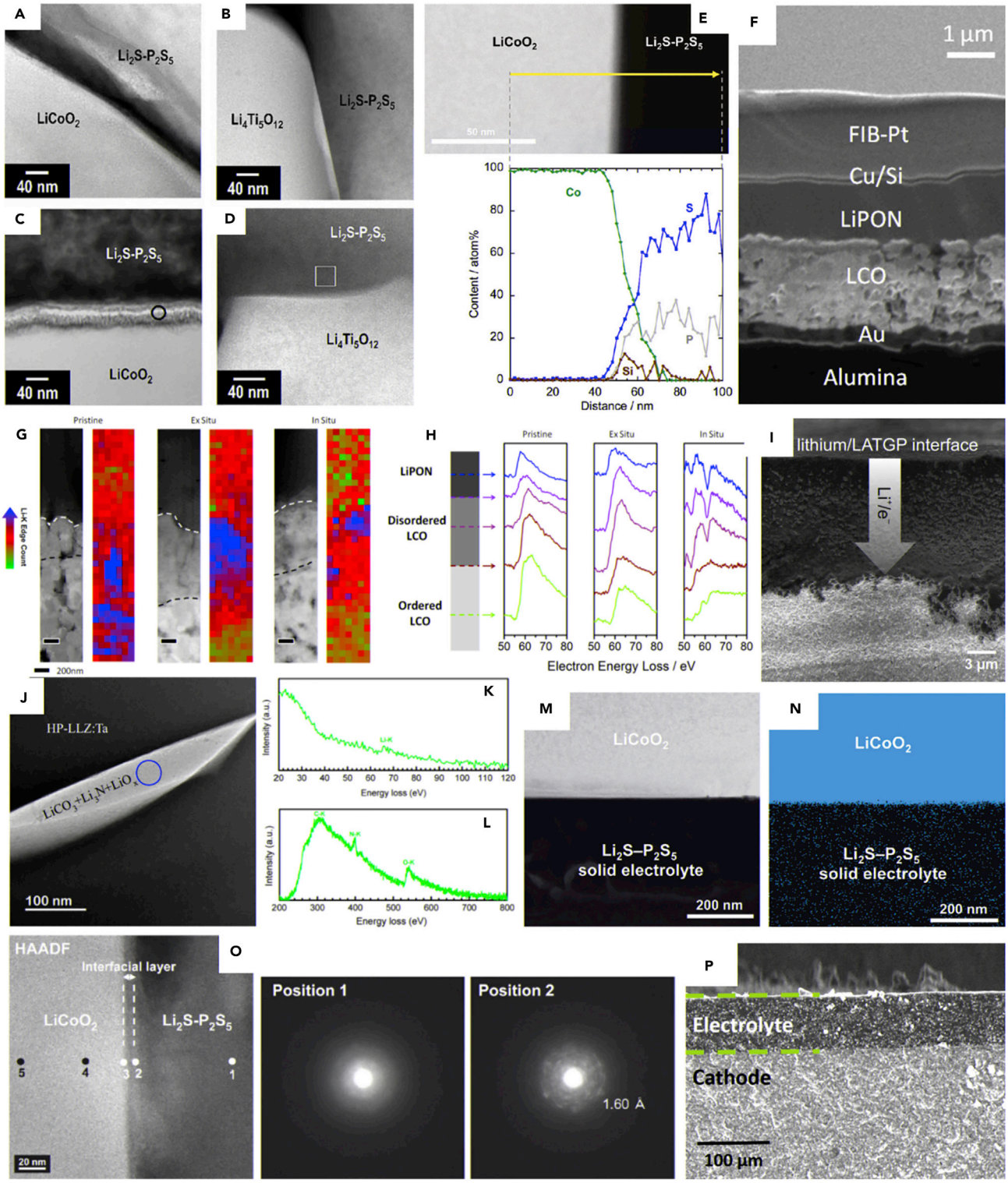

Figure 7. Selection of Images Obtained via Various Microscopic Methods

(A–D) HAADF-STEM images of the electrode-electrolyte interfaces. Reprinted from Kitaura et al.,[74] with permission. Copyright 2011, Royal Society of Chemistry.

(E) HAADF-STEM and linear EDX images of the Co element near the $LiCoO_2$ electrode/Li_2S-P_2S_5 solid-electrolyte interface. Reprinted from Sakuda et al.,[73] with permission. Copyright 2010, American Chemical Society.

Figure 7. *Continued*

(F–H) STEM (F) and STEM-EELS (G and H) images of the nano battery stack along with Li k-edge concentration mapping. Reprinted from Wang et al.,[75] with permission. Copyright 2016, American Chemical Society.

(I) Scanning EM cross-section image of an LATGP sample after approximately 12 hr contact with Li metal. LATGP stands for Li-Al-Ti-Ge-P-O electrolyte. Reprinted from Hartmann et al.,[38] with permission. Copyright 2013, American Chemical Society.

(J–L) High-resolution transmission electron microscopy (HRTEM) (J) and EELS (K and L) images of HP-LLZ:Ta (hot-pressed Ta-substituted $Li_7La_3Zr_2O_{12}$), where Li_3N, Li_2CO_3, and LiO_x were found along the grain boundaries. Reprinted from Tsai et al.,[76] with permission. Copyright 2016, American Chemical Society.

(M–O) HAADF-SEM (M), EDX (N), and SAED pattern (O) images of the Co element near the $LiCoO_2$ electrode/Li_2S-P_2S_5 solid-electrolyte interface. Reprinted from Sakuda et al.,[73] with permission. Copyright 2010, American Chemical Society.

(P) Scanning EM image of the interface between composite cathode containing 15 wt% polymer and the composite electrolyte. Reprinted from Chen et al.,[72] with permission. Copyright 2017, American Chemical Society.

in sodium-ion batteries.[88] XPS also performs well in SSB interfacial detection. For example, *ex situ* XPS verified the decomposition of LGPS.[37,90] Furthermore, Janek and coworkers have conducted several investigations using *in situ* XPS to study metal/solid-electrolyte stability; moreover, several *in situ* XPS experiments have been reported to verify the electrolyte decomposition of various solid electrolytes such as LLTO,[41] NASICON structure electrolyte like LATP,[38] and $Li_7P_3S_{11}$.[91] The schematic diagram for the device is shown in Figures 8A and 8B, where Li is vaporized by an argon beam and deposited on the electrolyte surface. The Li can either be adjacent to the electrolyte sample or have a certain space relationship with the sample. This simple device allows the stability of the interfaces between a metal electrode and a solid electrolyte to be detected, and the decomposition will show the stability of the interface. It must be noted, however, that this work would be more useful if cycling full cells were used in the device.

Various modifications to XPS such as hard XPS and soft XPS have resulted in a much wider probing depth range that is also more sensitive than traditional XPS.[93] Another fascinating method that is being applied to the problem is nuclear magnetic resonance (NMR)[69,76] and *in situ* NMR.[92] As an example, Nakayama et al. first assembled *in situ* NMR to observe elemental distribution and determine the uneven electrolysis of anion components at the interface between a cathode and solid polymer electrolyte[92] (Figure 8C) due to the high sensitivity of the technique toward Li-ion transport in bulk battery materials. It should also be noted that Yu et al. tested the quantity of the Li ions spontaneously transported between the Li_6PS_5Br solid electrolyte and the Li_2S cathode by NMR (Figure 8D).[69] Yet another approach is provided by solid-state NMR using multi-phase battery materials—even for multiple electrode phases or a mixture of electrode and electrolyte phases—to measure the spontaneous Li-ion transfer between different Li-containing phases. This approach provides unique selectivity for charge transfer over phase boundaries, and offers complementary information with respect to interfacial behavior. Remarkably, the nondestructive, contactless nature of the technique makes NMR friendly to sample pretreatment.

According to studies devoted to calculating the interfacial stability and design of SSB materials, augmented by powerful characterizations of interfacial by-products,[36,73,94,95] numerous sulfide-based compounds have been fabricated with higher ionic conductivities. The Kanno group proposed that with the doping of germanium into Li_3PS_4, the conductivity of the electrolyte can be greatly increased.[22] As a result, several sulfide electrolytes with high ionic conductivity have been fabricated, such as $Li_{3.25}P_{0.75}Ge_{0.25}S_4$ (2.2×10^{-3} S cm^{-1})[96] and $Li_{10}GeP_2S_{12}$ (10^{-2} S cm^{-1}).[22] Based on this known relationship, other doping approaches, for instance using $Li_{9.54}Si_{1.74}P_{1.44}S_{11.7}Cl_{0.3}$ (25 mS cm^{-1})[42], have also been employed. Interfacial impedance has always hindered the development of

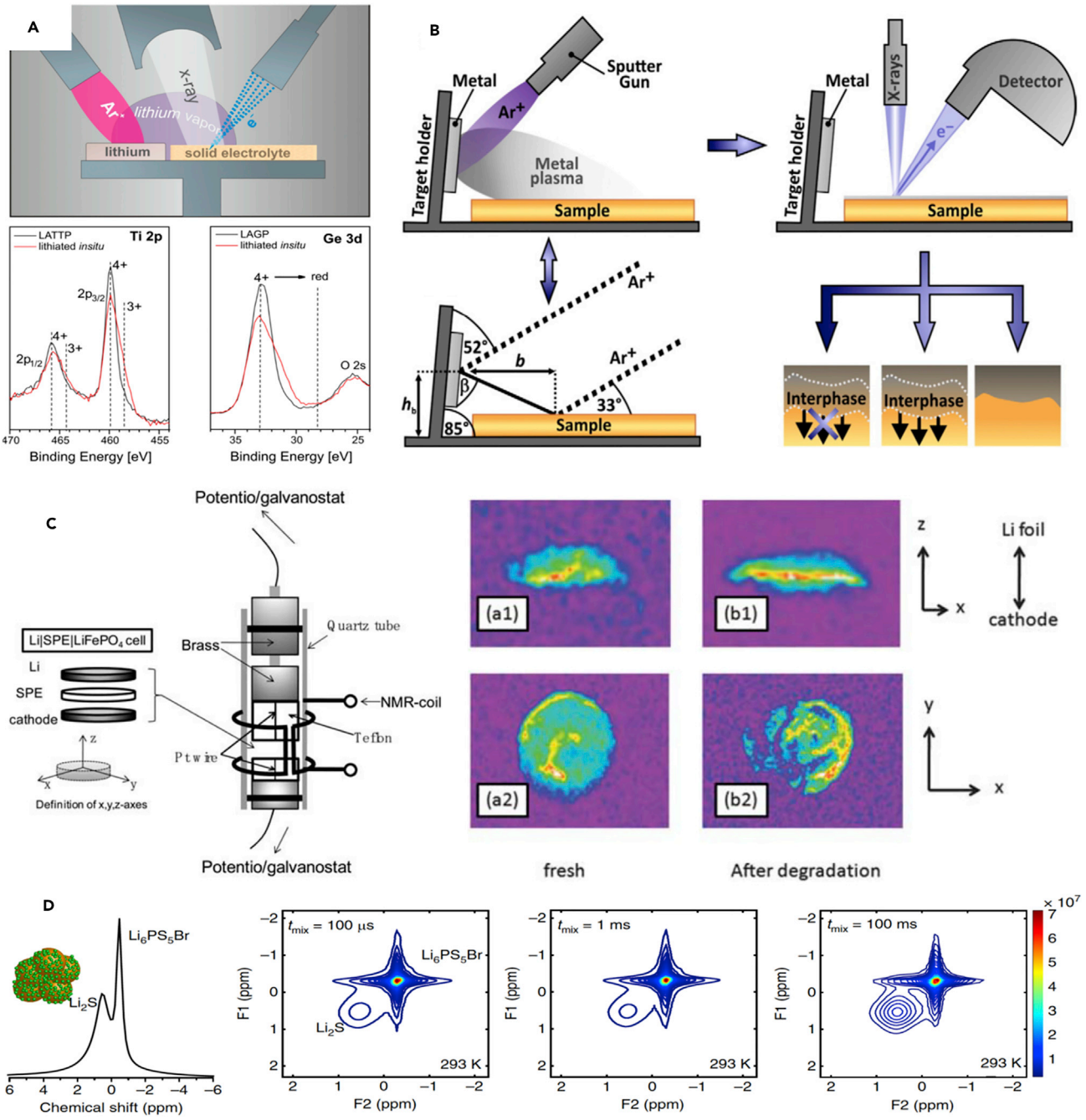

Figure 8. Selective Examples of Chemical Examinations

(A) *In situ* lithiation of solid electrolytes during XPS surface analysis. The argon ion gun is used to sputter a Li-metal foil placed in the vicinity of the sample of interest. Reprinted from Hartmann et al.,[38] with permission. Copyright 2013, American Chemical Society.

(B) The basic idea and setup of the *in situ* XPS technique. An argon ion beam is used to sputter lithium, gold, or aluminum metal on the sample surface. After deposition, the reaction products at the interface are investigated using photoelectron spectroscopy. Reprinted from Wenzel et al.,[41] with permission. Copyright 2015, Elsevier B.V.

(C) Schematic diagram of cell for *in situ* NMR imaging, and definition of x, y, and z axes of inserted Li polymer battery. Fluorine distribution in solid polymer electrolyte (SPE) measured by ^{19}F-NMR before (a1, a2) and after (b1, b2) electrochemical cycling. Reprinted from Nakayama et al.,[92] with permission. Copyright 2010, The Royal Society of Chemistry.

(D) NMR test result of the Li-ion transport between the Li_6PS_5Br solid electrolyte and the Li_2S cathode. Reprinted from Yu et al.,[69] with permission. Copyright 2017, Macmillan Publishers Limited.

SSBs featuring glass-ceramic electrolytes. To achieve close contact and good stability, the Tatsumisago group developed various interfacial modification methods. Coating the buffer layer on cathode materials represents a simple and effective way to soften the contact, and cathode coatings are known to improve the performance of high-voltage electrolytes by isolating the electrolyte materials from the low Li potential. Accordingly, Tatsumisago and colleagues coated a $LiCoO_2$ cathode with Li_4GeS_4-Li_3PS_4; the resulting solid-electrolyte coating formed a favorable and effective ion-conductive path to $LiCoO_2$ particles.[97] In another recent study, $50Li_4SiO_4 \cdot 50Li_3PO_4$ (mol%) film was coated on $LiCoO_2$ active material particles by PLD, with the coated electrolyte layer effectively decreasing interfacial resistance.[98] The mixing of metal oxides with Li_2S-P_2S_5 by mechanical milling can also enhance the stability of sulfide electrolyte in air. For example, combining a favorable metal oxide M_xO_y (M = Zn, Fe or Bi) with sulfide can decrease the Gibbs energy for H_2S formation, which is an effective way to improve the chemical stability of sulfide electrolytes.[99] Tatsumisago's group also described a heat-treatment method for improving ionic conductivity. They heated Li_2S-P_2S_5 glass ceramics to transform the particles into a dense material free from grain boundaries, which would decrease the porosity and the grain boundary resistance.[23]

Electrochemical Characterization

CV and electrochemical impedance spectroscopy (EIS) are two traditional electrochemical characterization approaches that focus on the entire battery, with each test performing a specific function. CV reports the current versus changing voltage to present a current-voltage graph, which provides information about chemical reactions and cycling reversibility. In contrast, EIS indicates the ionic impedance (high-frequency area) and the diffusion impedance (low-frequency area) of either a specific material or the overall cell (Figures 9A, 9H, and 9I).[22,100] The charge-discharge curves present the overall energy density and cycling reversibility, in which the plateaus correspond to the redox peaks in CV (Figures 9B and 9C).[22] The stability window of solid electrolytes can be characterized by CV. However, the stability window is usually overestimated by the traditional Li/solid electrolyte/inert metal cell test, in which the contact area between solid electrolyte and metal plate current collector is small, which results in slow kinetics of the electrolyte decomposition reaction. Han et al.[17] designed a novel Li/electrolyte/electrolyte-carbon cell composed of a mixture of carbon and solid electrolyte as the electrode to increase the contact area between electrolyte and current collector. This novel cell design can improve the electrolyte decomposition kinetics to a level similar to that of real SSBs. Their results show the intrinsic electrochemical stability window of LGPS to be only 1.7–2.1 V, which is much narrower than the window (0–5 V) characterized by traditional Li/solid electrolyte/inert metal cells.

In addition, symmetrical cells can be assembled to elucidate the details surrounding electrode-electrolyte interfacial contact via polarization testing. As illustrated in Figures 9E–9G and 9J,[100] this polarization test can be carried out via an electrode/electrolyte/electrode cell, and a set current can be run at certain temperature, whereby the overpotential refers to an additional IR drop. Similar testing was conducted by Luntz et al. in a prior context (Figures 3A–3D).[43] Recently, Wang et al. successfully distinguished the electronic conductivity and ionic conductivity of the materials by employing a combination of EIS and direct current polarization. Studies show that in ternary materials, with an increase in Ni content the activation energy of ion and electron conduction can be significantly reduced, which can improve the materials' electron-conduction and ion-conduction characteristics, and enhance the rate performance.[101] Moreover, the IR drop alone can provide sensitive information about

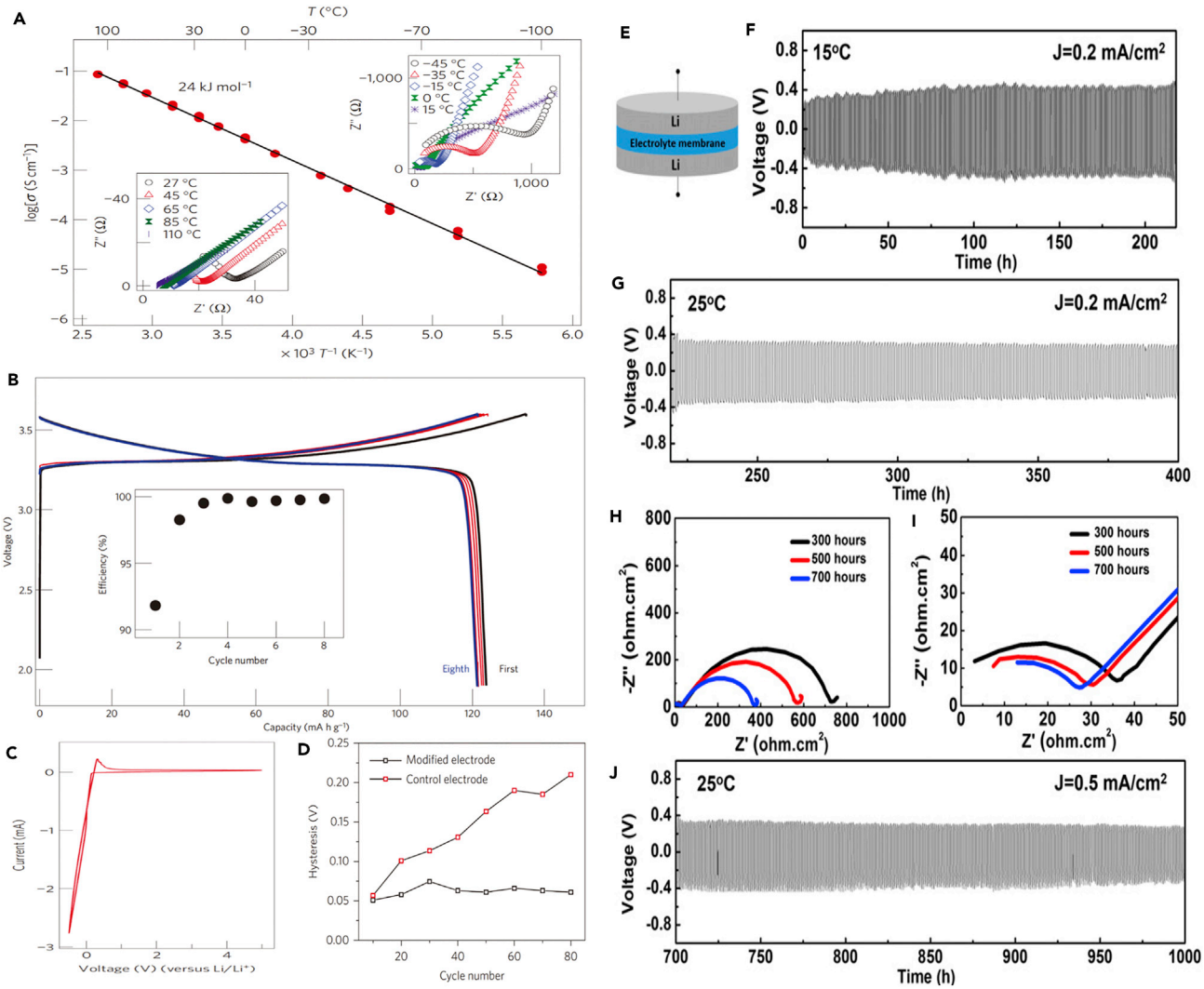

Figure 9. Selective Examples of Electrochemical Tests

(A–C) Impedance plots of the conductivity data from low to high temperatures and Arrhenius conductivity plots of $Li_{10}GeP_2S_{12}$ (A); charge-discharge curves of an all-solid-state battery consisting of $LiCoO_2$ cathode, $Li_{10}GeP_2S_{12}$ electrolyte, and In metal anode (B); and current-voltage curve of $Li/Li_{10}GeP_2S_{12}/Au$ cell (C). Reprinted from Kamaya et al.,[22] with permission. Copyright 2011, Macmillan Publishers Limited.

(D) Comparison of the hysteresis of Li deposition/dissolution for the modified electrode and the control electrode with Li metal as the reference/counter electrode. Reprinted from Zheng et al.,[11] with permission. Copyright 2014, Macmillan Publishers Limited.

(E–J) Schematic of symmetrical cell (E), EIS (H and I), and polarization test (F, G, and J) of the symmetric Li/FRPC (fiber-reinforced polymer composite) electrolyte/Li cell.

the interfacial connection (Figure 9D).[11] As the IR drop is an indication of resistance, a stable IR drop would indicate relatively stable interfacial contact; conversely, a severe IR drop change points to a change in contact circumstances.

Other Advanced Techniques

In addition to the aforementioned standard assessment approaches, a number of unconventional, yet interesting, experiments have been conducted. These include real-time thickness measurements,[92] thermogravimetric analysis,[102] differential scanning calorimetry, accelerated rate calorimetry, temperature programmed desorption, and atomic absorption spectroscopy. Here, we would like to provide a short introduction to two unique characterization techniques: (1) vibrational

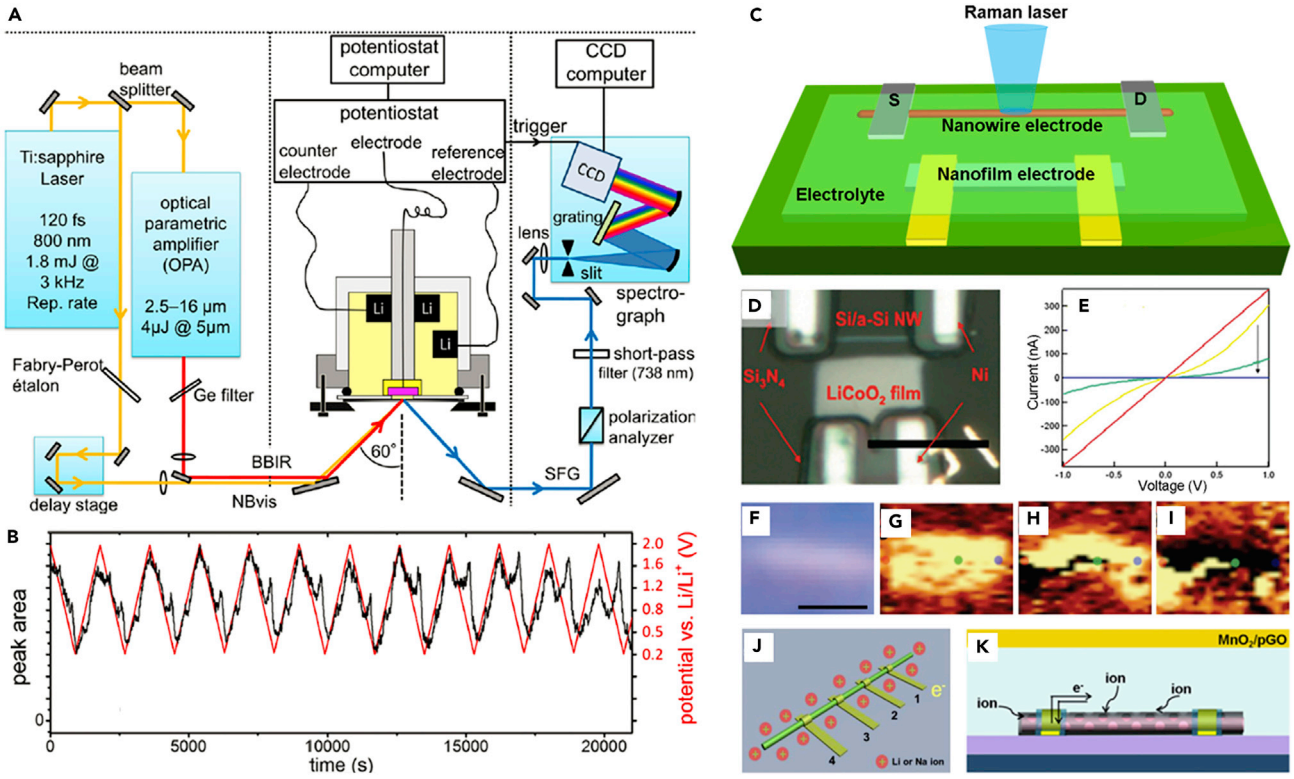

Figure 10. VSFG and On-Chip Single-Nanowire Battery Characterizations

(A) Schematic of the spectroelectrochemical apparatus.

(B) Potential-dependent SFG intensities of the carbonyl stretch during 12 CV cycles. Red lines denote the potential ramp. Reprinted from Nicolau et al.,[105] with permission. Copyright 2015, American Chemical Society.

(C) Schematic of a chip-based single-nanowire solid-state battery. In this schematic, a single nanowire is the cathode (or anode) and nanofilm is the anode (or cathode). A solid-state electrolyte thin film is coated on top of the chip. "S" indicates the source electrode and "D" indicates the drain electrode for nanowire conductance characterization.

(D) Optical microscopy image of a representative single-nanowire battery. Single Si/a-Si core/shell nanowire is the anode and $LiCoO_2$ film is the cathode. Scale bar represents 10 μm.

(E) *In situ* conductance characterization of a Si/a-Si nanowire at different charge/discharge states: red, primary state/100; yellow, after first charge and discharge; green, after second charge; blue, after second discharge.

(F–I) *In situ* Raman mapping of a Si/a-Si nanowire at different charge/discharge states. (F) Optical microscopy image; (G) primary state; (H) after first cycle; (I) after second cycle. Scale bar represents 2 μm.

(J) Schematic of a single-nanowire electrode with multicontacts for ion-transport study. Reprinted from Xu et al.,[113] with permission. Copyright 2015, American Chemical Society.

(K) Schematic of a porous graphene-wrapped single-nanowire electrode to improve electron and ion transport. Reprinted from Hu et al.,[114] with permission. Copyright 2016, American Chemical Society.

(C) to (I) reprinted from Mai et al.,[112] with permission. Copyright 2010, American Chemical Society.

sum-frequency generation spectroscopy and (2) on-chip single-nanowire battery characterization.

Vibrational Sum-Frequency Generation Spectroscopy. Vibrational sum-frequency generation spectroscopy (VSFG) has been proved to be a unique and effective chemical characterization technique for molecular interfaces (Figure 10A).[103] A number of advantages—such as interfacial specificity, high sensitivity, no vacuum requirement, real-time results, and *in situ* detection—have enabled VSFG to perform nondestructive characterizations in many fields. VSFG has been applied to various materials and interfaces such as polymers,[104] electrodes,[105,106] bio-membranes,[107] DNA,[108,109] and proteins.[110,111] To elucidate the SEI formation

mechanism in LIB liquid-electrolyte batteries, Mukherjee et al. designed an *in situ* VSFG device to monitor molecular changes[106] during CV cycling. Despite the fact that the signal contributions from the electrode interface and the diffuse layer electrolyte cannot be easily separated,[112] gradual changes in the VSFG signals in the carbonyl region were observed during potential cycling and the Li deposition/stripping at the anode (Figure 10B). It is clearly shown that dilithium ethylene glycol dicarbonate (LiEDC) molecules were formed after the sixth potential forward-backward scanning cycle. By monitoring the SFG intensity modulations of the -CH scissoring mode of LiEDC, and the -CH_2 wagging mode of tetrahydrofuran during the potential scanning cycle, the molecular mechanisms involved in SEI formation can be elucidated. In short, these results confirm that VSFG is capable of monitoring Li deposition and Li stripping during the potential scan. After successful demonstration of potential-dependent VSFG characterizations, the application of VSFG on other types of electrode interfaces can also be expected. It must be noted, however, that the requirements for Raman/infrared reactivity, non-centrosymmetrical structure, and light accessibility will limit the application of VSFG on certain interfaces. Indeed, there will certainly be more challenges in applying *in situ* VSFG characterization to SSB systems, in that they require special optical design for propagation of incident lights and collecting SFG signals. Accordingly, we would like to suggest more collaborative efforts toward this experimental goal.

On-Chip Single-Nanowire Battery Characterization. An on-chip single-nanowire battery could serve as a unique platform for *in situ* characterization of electron/ion transport and structure evolution in a battery. Mai et al.[112] described the development of a single-nanowire solid-state Li-ion battery to conduct *in situ* probing of the intrinsic reason for capacity fading. In this device (Figure 10C), a single nanowire serves as the cathode (or anode) and a nanofilm serves as the anode (or cathode). The nanowire and nanofilm are then put into contact with micro-/nanoscale metal electrodes, respectively, which have dual functions as current collectors during battery cycling and source/drain contacts during nanowire conductance characterization. Both the cathode and anode are fabricated on the same chip and wired up with the outer electric circuit without adding conductive additives or a binder. A solid-state electrolyte is deposited on top of the chip. To achieve *in situ* characterization, one could carry out battery cycling, nanowire conductance monitoring, and Raman mapping characterization simultaneously on this chip-based battery. Figure 10D shows an optical microscopy image of a representative single-nanowire battery. A single silicon nanowire is the anode, a $LiCoO_2$ nanofilm is the cathode, nickel microelectrodes serve as current collectors and source/drain contacts, and a polyethylene oxide-based solid-electrolyte film is coated on the chip. *In situ* current versus voltage (*I-V*) characterization shows that the conductance of silicon nanowire continuously decreases during charge/discharge cycling (Figure 10E). Specifically, the conductance decreases over two orders of magnitude after one cycle, which agrees with the *ex situ I-V* characterization of silicon nanowires described in the literature.[9] We also note that the *I-V* curves become nonlinear after charge/discharge cycling, indicating that the contacts of silicon nanowire and nickel current collectors also degrade during the electrochemical reaction, which cannot be easily confirmed using other characterization techniques. *In situ* Raman mapping reveals the inhomogeneous degradation of silicon nanowires during battery cycling (Figures 10F–10I), which results from amorphous Li-Si alloy formation. Another example involving $H_2V_3O_8$ nanowire as the cathode and graphene as the anode has been investigated on the basis of this single-nanowire battery platform.[112] Interestingly, unlike silicon, the conductance of a $H_2V_3O_8$ nanowire decreases after shallow discharge but can be recovered after shallow charge. However, the conductance

of a $H_2V_3O_8$ nanowire permanently decreases after deep discharge and charge. Taken together, these findings confirm that conductance decrease and the structural degradation of electrodes represent the two key issues leading to capacity fading.

The concept of this single-nanowire battery can be further extended with improved nanowire electrode design. Mai and colleagues can be credited for two improved design advancements: (1) multicontacts for ion transport (Figure 10J) and (2) porous graphene-wrapped nanowires to improve electron and ion transport (Figure 10K).[113,114] In brief, fabricating multiple metal microelectrodes on a single nanowire can enable one to record the conductance change of different sections of a single nanowire, thereby revealing ion transport characteristics along the nanowire (Figure 10J). Porous graphene wrapping on a single nanowire will not only improve electronic conductance but will also maintain efficient ion transport at the interface between the nanowire electrode and the electrolyte, while a dense solid graphene film coating hinders ion transport between the two (Figure 10K). These two improved single-nanowire battery designs could potentially be combined with newly developed micro-/nanoscale solid-state electrolyte patterns[115] to fabricate more advanced on-chip micro-/nanoscale SSB for comprehensive *in situ* characterizations.

Conclusion and Perspectives

In this review we present the challenges associated with interfaces in SSBs, discuss different types of solid-solid interfaces, and review a range of advanced characterization techniques. The challenges involving solid-solid interfaces can be generally summarized as those pertaining to physical contact and chemical contact. Specifically, two issues of interest involving physical contact are (1) the point contact between the electrolytes and electrodes that limits ionic transport, and (2) volume changes during battery cycling that could result in contact failure. In contrast, problems pertaining to chemical contact principally refer to side reactions between electrolyte and electrodes, which significantly decrease the stability and increase interfacial resistance. In short the major solid-solid interfaces consist of cathode-electrolyte interface, anode-electrolyte interface, and interparticle interface. For a cathode-electrolyte interface, the formation of a highly resistive interphase and/or a Li-depleted layer at the interface between the sulfide electrolyte and the high-voltage cathode represents a critical problem. For an anode-electrolyte interface, the major issue is Li dendrite growth and penetration through solid electrolyte, coupled with the side reactions between the sulfide electrolyte and Li anode. Interparticle interface should also not be neglected because continuous and efficient ionic and electronic transport paths within composite electrodes are difficult to achieve simultaneously. In addition, contact loss at the interfaces caused by the volume variation of electrode materials during electrochemical cycling represents a pervasive problem. It should be noted that even a slight volume change in intercalation-type materials would lead to severe contact failure in SSBs, which is a more serious issue for alloy and conversion-type materials. Although a theoretical study could provide a more nuanced understanding of the issues surrounding solid-solid interface, advanced characterization techniques must be developed to determine the required evidence experimentally. In particular, essential characterization techniques include microscopy observation, chemical composition analysis, and electrochemical characterization.

On the basis of current knowledge surrounding interfaces in SSBs, we would like to suggest some additional avenues for investigation. First, although a variety of advanced characterization techniques have successfully determined important

mechanisms associated with interfaces, most of them are *ex situ* characterizations that do not offer sufficient real-time information. In contrast, *in situ/operando* methods should be utilized to obtain a fundamental understanding of the composition and structures of interfaces, both of which are critical for designing SSBs. The challenge for an *in situ* study is that the solid-solid interfaces are embedded in SSBs, making it difficult to separate them (e.g., in liquid-electrolyte batteries). Thus, on the one hand the rational design of battery configurations to expose the interfaces at the micro-/nanoscale level should be considered for high-resolution characterization in the laboratory. On the other hand, nondestructive characterization techniques such as X-ray computed tomography could be very promising for revealing the inner interfaces for scanning and tracking SSBs in industry. Second, some applications rely on excellent power density only, while other applications just require high-energy density. Thus, SSBs must be designed to meet the needs of a broad range of applications, as it is unrealistic to assume that one type of battery will satisfy all the high-performance requirements/parameters seen in industry. For example, fine-tuning the ratio of active electrode particles and electrolyte particles within a composite electrode could determine whether it is high-energy density or high-power density.[116] Third, in addition to metal ions, metal-air[117] and metal-sulfur[118] systems featuring much higher energy density should also be investigated for use in SSBs. Last but not least, an important advantage of SSBs versus liquid-electrolyte batteries is that SSBs are more feasible for miniaturization. Thus, SSBs exhibit great potential for integration with microelectronic circuits—for example, in the development of self-powered micro-/nanoscale biological sensors.[119]

ACKNOWLEDGMENTS

Y.-C.C. acknowledges funding from the 4th Yellow Crane Talent Program of Wuhan City (08010004). C.L. acknowledges funding from China NSF (51703081). L.M. acknowledges funding from the National Natural Science Fund for Distinguished Young Scholars (51425204), National Key Research and Development Program of China (2016YFA0202603), the National Basic Research Program of China (2013CB934103), the Program of Introducing Talents of Discipline to Universities (B17034), the Yellow Crane Talent (Science & Technology) Program of Wuhan City, the National Natural Science Foundation of China (51521001), and the Fundamental Research Funds for the Central Universities (WUT: 2016III001, 2017III009). L.X. acknowledges support from the Fundamental Research Funds for the Central Universities (WUT: 2018IVA091).

AUTHOR CONTRIBUTIONS

Y.-C.C. and L.M. proposed the topic of the manuscript. L.X., S.T., Y.C., and K.W. wrote the manuscript. Y.-C.C., L.M., L.X., S.T., Y.C., K.W., J.L., C.L., and F.W. discussed and revised the manuscript. L.X., S.T., Y.C., and K.W. contributed equally to this work.

REFERENCES

1. Goodenough, J.B., and Park, K.-S. (2013). The Li-ion rechargeable battery: a perspective. J. Am. Chem. Soc. *135*, 1167–1176.

2. Choi, J.W., and Aurbach, D. (2016). Promise and reality of post-lithium-ion batteries with high energy densities. Nat. Rev. Mater. *1*, 16013.

3. Armand, M., and Tarascon, J.-M. (2008). Building better batteries. Nature *451*, 652–657.

4. Bruce, P.G., Freunberger, S.A., Hardwick, L.J., and Tarascon, J.-M. (2012). Li-O_2 and Li-S batteries with high energy storage. Nat. Mater. *11*, 19–29.

5. Ottakam Thotiyl, M.M., Freunberger, S.A., Peng, Z., Chen, Y., Liu, Z., and Bruce, P.G. (2013). A stable cathode for the aprotic Li-O_2 battery. Nat. Mater. *12*, 1050–1056.

6. Cheng, X.-B., Zhang, R., Zhao, C.-Z., and Zhang, Q. (2017). Toward safe lithium metal anode in rechargeable batteries: a review. Chem. Rev. *117*, 10403–10473.

7. Peng, H.-J., Huang, J.-Q., and Zhang, Q. (2017). A review of flexible lithium-sulfur and analogous alkali metal-chalcogen rechargeable batteries. Chem. Soc. Rev. *46*, 5237–5288.

8. Xu, R., Lu, J., and Amine, K. (2015). Progress in mechanistic understanding and

characterization techniques of Li-S batteries. Adv. Energy Mater. *5*, 1500408.

9. Chan, C.K., Peng, H., Liu, G., McIlwrath, K., Zhang, X., Huggins, R.A., and Cui, Y. (2008). High-performance lithium battery anodes using silicon nanowires. Nat. Nanotechnol. *3*, 31–35.

10. Wu, H., Chan, G., Choi, J.W., Ryu, I., Yao, Y., McDowell, M.T., Lee, S.W., Jackson, A., Yang, Y., Hu, L., et al. (2012). Stable cycling of double-walled silicon nanotube battery anodes through solid-electrolyte interphase control. Nat. Nanotechnol. *7*, 310–315.

11. Zheng, G., Lee, S.W., Liang, Z., Lee, H.-W., Yan, K., Yao, H., Wang, H., Li, W., Chu, S., and Cui, Y. (2014). Interconnected hollow carbon nanospheres for stable lithium metal anodes. Nat. Nanotechnol. *9*, 618–623.

12. Li, B., Li, S., Xu, J., and Yang, S. (2016). A new configured lithiated silicon-sulfur battery built on 3D graphene with superior electrochemical performances. Energy Environ. Sci. *9*, 2025–2030.

13. Chung, S.-H., Chang, C.-H., and Manthiram, A. (2016). A core-shell electrode for dynamically and statically stable Li-S battery chemistry. Energy Environ. Sci. *9*, 3188–3200.

14. Liu, J., Galpaya, D.G.D., Yan, L., Sun, M., Lin, Z., Yan, C., Liang, C., and Zhang, S. (2017). Exploiting a robust biopolymer network binder for an ultrahigh-areal-capacity Li-S battery. Energy Environ. Sci. *10*, 750–755.

15. Huggins, R.A., and Boukamp, B.A. (1981). All-solid electrodes with mixed conductor matrix. J. Electrochem. Soc. *128*, 725–729.

16. Wang, Y., Richards, W.D., Ong, S.P., Miara, L.J., Kim, J.C., Mo, Y., and Ceder, G. (2015). Design principles for solid-state lithium superionic conductors. Nat. Mater. *14*, 1026–1031.

17. Han, F., Zhu, Y., He, X., Mo, Y., and Wang, C. (2016). Electrochemical stability of $Li_{10}GeP_2S_{12}$ and $Li_7La_3Zr_2O_{12}$ solid electrolytes. Adv. Energy Mater. *6*, 1501590.

18. Takeda, Y., Yamamoto, O., and Imanishi, N. (2016). Lithium dendrite formation on a lithium metal anode from liquid, polymer and solid electrolytes. Electrochemistry *84*, 210–218.

19. Yang, C., Fu, K., Zhang, Y., Hitz, E., and Hu, L. (2017). Protected lithium-metal anodes in batteries: from liquid to solid. Adv. Mater. *29*, 1701169.

20. Monroe, C., and Newman, J. (2005). The impact of elastic deformation on deposition kinetics at lithium/polymer interfaces. J. Polym. Sci. *152*, A396–A404.

21. Janek, J., and Zeier, W.G. (2016). A solid future for battery development. Nat. Energy *1*, 16141.

22. Kamaya, N., Homma, K., Yamakawa, Y., Hirayama, M., Kanno, R., Yonemura, M., Kamiyama, T., Kato, Y., Hama, S., Kawamoto, K., et al. (2011). A lithium superionic conductor. Nat. Mater. *10*, 682–686.

23. Seino, Y., Ota, T., Takada, K., Hayashi, A., and Tatsumisago, M. (2014). A sulphide lithium super ion conductor is superior to liquid ion conductors for use in rechargeable batteries. Energy Environ. Sci. *7*, 627–631.

24. Takada, K., Aotani, N., Iwamoto, K., and Kondo, S. (1996). Solid state lithium battery with oxysulfide glass. Solid State Ionics *86*, 877–882.

25. Yan, K., Lu, Z., Lee, H.-W., Xiong, F., Hsu, P.-C., Li, Y., Zhao, J., Chu, S., and Cui, Y. (2016). Selective deposition and stable encapsulation of lithium through heterogeneous seeded growth. Nat. Energy *1*, 16010.

26. Goodenough, J.B., and Kim, Y. (2010). Challenges for rechargeable Li batteries. Chem. Mater. *22*, 587–603.

27. Verma, P., Maire, P., and Novak, P. (2010). A review of the features and analyses of the solid electrolyte interphase in Li-ion batteries. Electrochim. Acta *55*, 6332–6341.

28. An, S.J., Li, J., Daniel, C., Mohanty, D., Nagpure, S., and Wood, D.L. (2016). The state of understanding of the lithium-ion-battery graphite solid electrolyte interphase (SEI) and its relationship to formation cycling. Carbon *105*, 52–76.

29. Wang, A., Kadam, S., Li, H., Shi, S., and Qi, Y. (2018). Review on modeling of the anode solid electrolyte interphase (SEI) for lithium-ion batteries. npj Comput. Mater. *4*, 15.

30. Cheng, X.-B., Zhang, R., Zhao, C.-Z., Wei, F., Zhang, J.-G., and Zhang, Q. (2016). A review of solid electrolyte interphases on lithium metal anode. Adv. Sci. *3*, 1500213.

31. Porz, L., Swamy, T., Sheldon, B.W., Rettenwander, D., Frömling, T., Thaman, H.L., Berendts, S., Uecker, R., Carter, W.C., and Chiang, Y.-M. (2017). Mechanism of lithium metal penetration through inorganic solid electrolytes. Adv. Energy Mater. *7*, 1701003.

32. Hu, Y.-S. (2016). Batteries: getting solid. Nat. Energy *1*, 16042.

33. Takada, K. (2013). Progress and prospective of solid-state lithium batteries. Acta Mater. *61*, 759–770.

34. Zhu, Y., He, X., and Mo, Y. (2015). Origin of outstanding stability in the lithium solid electrolyte materials: insights from thermodynamic analyses based on first-principles calculations. ACS Appl. Mater. Interfaces *7*, 23685–236893.

35. Zhu, Y., He, X., and Mo, Y. (2016). First principles study on electrochemical and chemical stability of solid electrolyte-electrode interfaces in all-solid-state Li-ion batteries. J. Mater. Chem. A *4*, 3253–3266.

36. Oh, G., Hirayama, M., Kwon, O., Suzuki, K., and Kanno, R. (2016). Bulk-type all solid-state batteries with 5 V class $LiNi_{0.5}Mn_{1.5}O_4$ cathode and $Li_{10}GeP_2S_{12}$ solid electrolyte. Chem. Mater. *28*, 2634–2640.

37. Wenzel, S., Randau, S., Leichtweiss, T., Weber, D.A., Sann, J., Zeier, W.G., and Janek, J. (2016). Direct observation of the interfacial instability of the fast ionic conductor $Li_{10}GeP_2S_{12}$ at the lithium metal anode. Chem. Mater. *28*, 2400–2407.

38. Hartmann, P., Leichtweiss, T., Busche, M.R., Schneider, M., Reich, M., Sann, J., Adelhelm, P., and Janek, J. (2013). Degradation of NASICON-type materials in contact with lithium metal: formation of mixed conducting interphases (MCI) on solid electrolytes. J. Phys. Chem. C *117*, 21064–21074.

39. Schwobel, A., Hausbrand, R., and Jaegermann, W. (2015). Interface reactions between LiPON and lithium studied by *in-situ* X-ray photoemission. Solid State Ionics *273*, 51–54.

40. Wolfenstine, J., Allen, J.L., Read, J., and Sakamoto, J. (2013). Chemical stability of cubic $Li_7La_3Zr_2O_{12}$ with molten lithium at elevated temperature. J. Mater. Sci. *48*, 5846–5851.

41. Wenzel, S., Leichtweiss, T., Krüger, D., Sann, J., and Janek, J. (2015). Interphase formation on lithium solid electrolytes—an *in situ* approach to study interfacial reactions by photoelectron spectroscopy. Solid State Ionics *278*, 98–105.

42. Kato, Y., Hori, S., Saito, T., Suzuki, K., Hirayama, M., Mitsui, A., Yonemura, M., Iba, H., and Kanno, R. (2016). High-power all-solid-state batteries using sulfide superionic conductors. Nat. Energy *1*, 16030.

43. Luntz, A.C., Voss, J., and Reuter, K. (2015). Interfacial challenges in solid-state Li ion batteries. J. Phys. Chem. Lett. *6*, 4599–4604.

44. Ohta, S., Kobayashi, T., Seki, J., and Asaoka, T. (2012). Electrochemical performance of an all-solid-state lithium ion battery with garnet-type oxide electrolyte. J. Power Sources *202*, 332–335.

45. Nam, Y.J., Cho, S.J., Oh, D.Y., Lim, J.M., Kim, S.Y., Song, J.H., Lee, Y.G., Lee, S.Y., and Jung, Y.S. (2015). Bendable and thin sulfide solid electrolyte film: a new electrolyte opportunity for free-standing and stackable high-energy all-solid-state lithium-ion batteries. Nano Lett. *15*, 3317–3323.

46. Han, F., Yue, J., Chen, C., Zhao, N., Fan, X., Ma, Z., Gao, T., Wang, F., Guo, X., and Wang, C. (2018). Interphase engineering enabled all-ceramic lithium battery. Joule *2*, 497–508.

47. Haruyama, J., Sodeyama, K., Han, L., Takada, K., and Tateyama, Y. (2014). Space-charge layer effect at interface between oxide cathode and sulfide electrolyte in all-solid-state lIithium-ion battery. Chem. Mater. *26*, 4248–4255.

48. Takada, K., Ohta, N., Zhang, L.Q., Fukuda, K., Sakaguchi, I., Ma, R., Osada, M., and Sasaki, T. (2008). Interfacial modification for high-power solid-state lithium batteries. Solid State Ionics *179*, 1333–1337.

49. Ohta, N., Takada, K., Zhang, L., Ma, R., Osada, M., and Sasaki, T. (2006). Enhancement of the high-rate capability of solid-state lithium batteries by nanoscale interfacial modification. Adv. Mater. *18*, 2226–2229.

50. Ohta, N. (2007). $LiNbO_3$-coated $LiCoO_2$ as cathode material for all solid-state lithium secondary batteries. Electrochem. Commun. *9*, 1486–1490.

51. Takada, K., Ohta, N., Zhang, L., Xu, X., Hang, B.T., Ohnishi, T., Osada, M., and Sasaki, T.

(2012). Interfacial phenomena in solid-state lithium battery with sulfide solid electrolyte. Solid State Ionics *225*, 594–597.

52. Koerver, R., Aygün, I., Leichtweiß, T., Dietrich, C., Zhang, W., Binder, J.O., Hartmann, P., Zeier, W.G., and Janek, J. (2017). Capacity fade in solid-state batteries: interphase formation and chemomechanical processes in nickel-rich layered oxide cathodes and lithium thiophosphate solid electrolytes. Chem. Mater. *29*, 5574–5582.

53. Zhang, W., Leichtweiss, T., Culver, S.P., Koerver, R., Das, D., Weber, D.A., Zeier, W.G., and Janek, J. (2017). The detrimental effects of carbon additives in $Li_{10}GeP_2S_{12}$-based solid-state batteries. ACS Appl. Mater. Interfaces *9*, 35888–35896.

54. Monroe, C., and Newman, J. (2004). The effect of interfacial deformation on electrodeposition kinetics. J. Electrochem. Soc. *151*, A880–A886.

55. Xu, K., Von, C.A., and Lee, U. (2010). Differentiating contributions to "ion transfer" barrier from interphasial resistance and Li^+ desolvation at electrolyte/graphite interface. Langmuir *26*, 11538–11543.

56. Liu, X., Deng, X., Liu, R., Yan, H., Guo, Y., Wang, D., and Wan, L. (2014). Single nanowire electrode electrochemistry of silicon anode by *in situ* atomic force microscopy: solid electrolyte interphase growth and mechanical properties. ACS Appl. Mater. Interfaces *6*, 20317–20323.

57. Zhang, J., Wang, R., Yang, X., Lu, W., Wu, X., Wang, X., Li, H., and Chen, L. (2012). Direct observation of inhomogeneous solid electrolyte interphase on MnO anode with atomic force microscopy and spectroscopy. Nano Lett. *12*, 2153–2157.

58. Pei, A., Zheng, G., Shi, F., Li, Y., and Cui, Y. (2017). Nanoscale nucleation and growth of electrodeposited lithium metal. Nano Lett. *17*, 1132–1139.

59. Yang, Y., Jeong, S., Hu, L., Wu, H., Lee, S.W., and Cui, Y. (2011). Transparent lithium-ion batteries. Proc. Natl. Acad. Sci. USA *108*, 13013–13018.

60. Wang, S., Xu, J., Wang, W., Wang, G.-J.N., Rastak, R., Molina-Lopez, F., Chung, J.W., Niu, S., Feig, V.R., and Lopez, J. (2018). Skin electronics from scalable fabrication of an intrinsically stretchable transistor array. Nature *555*, 83–88.

61. Appetecchi, G., Croce, F., Persi, L., Ronci, F., and Scrosati, B. (2000). Transport and interfacial properties of composite polymer electrolytes. Electrochim. Acta *45*, 1481–1490.

62. Schulze, M.W., McIntosh, L.D., Hillmyer, M.A., and Lodge, T.P. (2014). High-modulus, high-conductivity nanostructured polymer electrolyte membranes via polymerization-induced phase separation. Nano Lett. *14*, 122–126.

63. Amanchukwu, C.V., Harding, J.R., Shao-Horn, Y., and Hammond, P.T. (2015). Understanding the chemical stability of polymers for lithium-air batteries. Chem. Mater. *27*, 550–561.

64. Stone, G.M., Mullin, S.A., Teran, A.A., Hallinan, J.D.T., Minor, A.M., Hexemer, A., and Balsara, N.P. (2012). Resolution of the modulus versus adhesion dilemma in solid polymer electrolytes for rechargeable lithium metal batteries. J. Electrochem. Soc. *159*, A222–A227.

65. Gao, H., Xue, L., Xin, S., Park, K., and Goodenough, J.B. (2017). A plastic-crystal electrolyte interphase for all-solid-state sodium batteries. Angew. Chem. Int. Ed. *56*, 5541–5545.

66. Strauss, F., Bartsch, T., de Biasi, L., Kim, A.Y., Janek, J., Hartmann, P., and Brezesinski, T. (2018). Impact of cathode material particle size on the capacity of bulk-type all-solid-state batteries. ACS Energy Lett. *3*, 992–996.

67. Sakuma, M., Suzuki, K., Hirayama, M., and Kanno, R. (2016). Reactions at the electrode/electrolyte interface of all-solid-state lithium batteries incorporating Li-M (M = Sn, Si) alloy electrodes and sulfide-based solid electrolytes. Solid State Ionics *285*, 101–105.

68. Yang, L., Wang, Z., Feng, Y., Tan, R., Zuo, Y., Gao, R., Zhao, Y., Han, L., Wang, Z., and Pan, F. (2017). Flexible composite solid electrolyte facilitating highly stable "soft contacting" Li-electrolyte interface for solid state lithium-ion batteries. Adv. Energy Mater. *7*, 1701437.

69. Yu, C., Ganapathy, S., Eck, E., Wang, H., Basak, S., Li, Z., and Wagemaker, M. (2017). Accessing the bottleneck in all-solid state batteries, lithium-ion transport over the solid-electrolyte-electrode interface. Nat. Commun. *8*, 1086.

70. Kato, T., Yoshida, R., Yamamoto, K., Hirayama, T., Motoyama, M., West, W.C., and Iriyama, Y. (2016). Effects of sintering temperature on interfacial structure and interfacial resistance for all-solid-state rechargeable lithium batteries. J. Power Sources *325*, 584–590.

71. Mai, L., Yan, M., and Zhao, Y. (2017). Track batteries degrading in real time. Nature *546*, 469.

72. Chen, R.-J., Zhang, Y.-B., Liu, T., Xu, B.-Q., Lin, Y.-H., Nan, C.-W., and Shen, Y. (2017). Addressing the interface issues in all-solid-state bulk-type lithium ion battery via an all-composite approach. ACS Appl. Mater. Interfaces *9*, 9654–9661.

73. Sakuda, A., Hayashi, A., and Tatsumisago, M. (2010). Interfacial observation between $LiCoO_2$ electrode and Li_2S-P_2S_5 solid electrolytes of all-solid-state lithium secondary batteries using transmission electron microscopy. Chem. Mater. *22*, 949–956.

74. Kitaura, H., Hayashi, A., Ohtomo, T., Hama, S., and Tatsumisago, M. (2011). Fabrication of electrode-electrolyte interfaces in all-solid-state rechargeable lithium batteries by using a supercooled liquid state of the glassy electrolytes. J. Mater. Chem. *21*, 118–124.

75. Wang, Z., Santhanagopalan, D., Zhang, W., Wang, F., Xin, H.L., He, K., Li, J., Dudney, N., and Meng, Y.S. (2016). *In situ* STEM-EELS observation of nanoscale interfacial phenomena in all-solid-state batteries. Nano Lett. *16*, 3760–3767.

76. Tsai, C.L., Roddatis, V., Chandran, C.V., Ma, Q., Uhlenbruck, S., Bram, M., Heitjans, P., and Guillon, O. (2016). $Li_7La_3Zr_2O_{12}$ interface modification for Li dendrite prevention. ACS Appl. Mater. Interfaces *8*, 10617–10626.

77. Brazier, A., Dupont, L., Dantras-Laffont, L., Kuwata, N., Kawamura, J., and Tarascon, J.M. (2008). First cross-section observation of an all solid-state lithium-Ion "nanobattery" by transmission electron microscopy. Chem. Mater. *20*, 2352–2359.

78. He, K., Bi, X., Yuan, Y., Foroozan, T., Song, B., Amine, K., Lu, J., and Shahbazian-Yassar, R. (2018). *Operando* liquid cell electron microscopy of discharge and charge kinetics in lithium-oxygen batteries. Nano Energy *49*, 338–345.

79. Santhanagopalan, D., Qian, D., McGilvray, T., Wang, Z., Wang, F., Camino, F., Graetz, J., Dudney, N., and Meng, Y.S. (2014). Interface limited lithium transport in solid-state batteries. J. Phys. Chem. Lett. *5*, 298–303.

80. Wang, F., Yu, H.-C., Chen, M.-H., Wu, L., Pereira, N., Thornton, K., Van der Ven, A., Zhu, Y., Amatucci, G.G., and Graetz, J. (2012). Tracking lithium transport and electrochemical reactions in nanoparticles. Nat. Commun. *3*, 1201.

81. Shen, C., Hu, G., Cheong, L.-Z., Huang, S., Zhang, J.-G., and Wang, D. (2018). Direct observation of the growth of lithium dendrites on graphite anodes by *operando* EC-AFM. Small Methods *2*, 1700298.

82. Tian, Y., Shi, T., Richards, W.D., Li, J., Kim, J.C., Bo, S.-H., and Ceder, G. (2017). Compatibility issues between electrodes and electrolytes in solid-state batteries. Energy Environ. Sci. *10*, 1150–1166.

83. Mo, Y., Ong, S.P., and Ceder, G. (2011). First principles study of the $Li_{10}GeP_2S_{12}$ lithium super ionic conductor material. Chem. Mater. *24*, 15–17.

84. Richards, W.D., Miara, L.J., Wang, Y., Kim, J.C., and Ceder, G. (2015). Interface stability in solid-state batteries. Chem. Mater. *28*, 266–273.

85. Kuhn, A., Kohler, J., and Lotsch, B.V. (2013). Single-crystal X-ray structure analysis of the superionic conductor $Li_{10}GeP_2S_{12}$. Phys. Chem. Chem. Phys. *15*, 11620–11622.

86. Zhang, H., Hao, S., and Lin, J. (2017). Influence of Li_2O-B_2O_3 glass on ionic migration and interfacial properties of $La_{2/3-x}$ $Li_{3x}TiO_3$ solid electrolyte. J. Alloy. Compd. *704*, 109–116.

87. Demir-Cakan, R., Morcrette, M., Gangulibabu, Gueguen, A., Dedryvere, R., and Tarascon, J.M. (2013). Li-S batteries: simple approaches for superior performance. Energy Environ. Sci. *6*, 176–182.

88. Ponrouch, A., Dedryvère, R., Monti, D., Demet, A.E., Ateba Mba, J.M., Croguennec, L., Masquelier, C., Johansson, P., and Palacín, M.R. (2013). Towards high energy density sodium ion batteries through electrolyte optimization. Energy Environ. Sci. *6*, 2361–2369.

89. Philippe, B., Dedryvere, R., Allouche, J., Lindgren, F., Gorgoi, M., Rensmo, H., Gonbeau, D., and Edstrom, K. (2012). Nanosilicon electrodes for lithium-ion batteries: interfacial mechanisms studied by

hard and soft X-ray photoelectron spectroscopy. Chem. Mater. *24*, 1107–1115.

90. Han, F., Gao, T., Zhu, Y., Gaskell, K.J., and Wang, C. (2015). A battery made from a single material. Adv. Mater. *27*, 3473–3483.

91. Wenzel, S., Weber, D.A., Leichtweiss, T., Busche, M.R., Sann, J., and Janek, J. (2016). Interphase formation and degradation of charge transfer kinetics between a lithium metal anode and highly crystalline $Li_7P_3S_{11}$ solid electrolyte. Solid State Ionics *286*, 24–33.

92. Nakayama, M., Wada, S., Kuroki, S., and Nogami, M. (2010). Factors affecting cyclic durability of all-solid-state lithium polymer batteries using poly(ethylene oxide)-based solid polymer electrolytes. Energy Environ. Sci. *3*, 1995–2002.

93. Malmgren, S., Ciosek, K., Hahlin, M., Gustafsson, T., Gorgoi, M., Rensmo, H., and Edström, K. (2013). Comparing anode and cathode electrode/electrolyte interface composition and morphology using soft and hard X-ray photoelectron spectroscopy. Electrochim. Acta *97*, 23–32.

94. Kobayashi, T., Yamada, A., and Kanno, R. (2008). Interfacial reactions at electrode/electrolyte boundary in all solid-state lithium battery using inorganic solid electrolyte, thio-LISICON. Electrochim. Acta *53*, 5045–5050.

95. Otoyama, M., Ito, Y., Hayashi, A., and Tatsumisago, M. (2016). Raman imaging for $LiCoO_2$ composite positive electrodes in all-solid-state lithium batteries using Li_2S-P_2S_5 solid electrolytes. J. Power Sources *302*, 419–425.

96. Kanno, R., Murayama, M., Inada, T., Kobayashi, T., Sakamoto, K., Sonoyama, N., Yamada, A., and Kondo, S. (2004). A self-assembled breathing interface for all-solid-state ceramic lithium batteries. Electrochem. Solid State Lett. *7*, A455–A458.

97. Ito, Y., Otoyama, M., Hayashi, A., Ohtomo, T., and Tatsumisago, M. (2017). Electrochemical and structural evaluation for bulk-type all-solid-state batteries using Li_4GeS_4-Li_3PS_4 electrolyte coating on $LiCoO_2$ particles. J. Power Sources *360*, 328–335.

98. Sakurai, Y., Sakuda, A., Hayashi, A., and Tatsumisago, M. (2011). Preparation of amorphous Li_4SiO_4-Li_3PO_4 thin films by pulsed laser deposition for all-solid-state lithium secondary batteries. Solid State Ionics *182*, 59–63.

99. Hayashi, A., Muramatsu, H., Ohtomo, T., Hama, S., and Tatsumisago, M. (2013). Improvement of chemical stability of Li_3PS_4 glass electrolytes by adding M_xO_y (M = Fe, Zn, and Bi) nanoparticles. J. Mater. Chem. A *1*, 6320–6326.

100. Fu, K., Gong, Y., Dai, J., Gong, A., Han, X., Yao, Y., Wang, C., Wang, Y., Chen, Y., Yan, C., et al. (2016). Flexible, solid-state, ion-conducting membrane with 3D garnet nanofiber networks for lithium batteries. Proc. Natl. Acad. Sci. USA *113*, 7094–7099.

101. Wang, S., Yan, M., Li, Y., Vinado, C., and Yang, J. (2018). Separating electronic and ionic conductivity in mix-conducting layered lithium transition-metal oxides. J. Power Sources *393*, 75–82.

102. Li, Y., Xu, B., Xu, H., Duan, H., Lu, X., Xin, S., Zhou, W., Xue, L., Fu, G., Manthiram, A., et al. (2017). Hybrid polymer/garnet electrolyte with a small interfacial resistance for lithium-ion batteries. Angew. Chem. Int. Ed. *56*, 753–756.

103. Wang, H., Gan, W., Lu, R., Rao, Y., and Wu, B. (2005). Quantitative spectral and orientational analysis in surface sum frequency generation vibrational spectroscopy (SFG-VS). Int. Rev. Phys. Chem. *24*, 191–256.

104. Chen, Z., Shen, Y.R., and Somorjai, G.A. (2002). Studies of polymer surfaces by sum frequency generation vibrational spectroscopy. Annu. Rev. Phys. Chem. *53*, 437–465.

105. Nicolau, B.G., García-Rey, N., Dryzhakov, B., and Dlott, D.D. (2015). Interfacial processes of a model lithium ion battery anode observed, *in situ*, with vibrational sum-frequency generation spectroscopy. J. Phys. Chem. C *119*, 10227–10233.

106. Mukherjee, P., Lagutchev, A., and Dlott, D.D. (2012). *In situ* probing of solid-electrolyte interfaces with nonlinear coherent vibrational spectroscopy. J. Electrochem. Soc. *159*, A244–A252.

107. Wei, F., Xiong, W., Li, W., Lu, W., Allen, H.C., and Zheng, W. (2015). Assembly and relaxation behaviours of phosphatidylethanolamine monolayers investigated by polarization and frequency resolved SFG-VS. Phys. Chem. Chem. Phys. *17*, 25114–25122.

108. Wei, F., Tian, K., and Zheng, W. (2015). Interfacial structure and transformation of guanine-rich oligonucleotides on solid supported lipid bilayer investigated by sum frequency generation vibrational spectroscopy. J. Phys. Chem. C *119*, 27038–27044.

109. Wang, L., Shen, Y., Yang, Y., Lu, W., Li, W., Wei, F., Zheng, G., Zhou, Y., Zheng, W., and Cao, Y. (2017). Stern-layer adsorption of oligonucleotides on lamellar cationic lipid bilayer investigated by polarization-resolved SFG-VS. ACS Omega *2*, 9241–9249.

110. Ye, S., Wei, F., Li, H., Tian, K., and Luo, Y. (2013). Structure and orientation of interfacial proteins determined by sum frequency generation vibrational spectroscopy: method and application. Adv. Protein Chem. Struct. Biol. *93*, 213–255.

111. Tan, J., Zhang, B., Luo, Y., and Ye, S. (2017). Ultrafast vibrational dynamics of membrane-bound peptides at the lipid bilayer/water interface. Angew. Chem. Int. Ed. *56*, 12977–12981.

112. Mai, L., Dong, Y., Xu, L., and Han, C. (2010). Single nanowire electrochemical devices. Nano Lett. *10*, 4273–4278.

113. Xu, X., Yan, M., Tian, X., Yang, C., Shi, M., Wei, Q., Xu, L., and Mai, L. (2015). *In Situ* investigation of Li and Na ion transport with single nanowire electrochemical devices. Nano Lett. *15*, 3879–3884.

114. Hu, P., Yan, M., Wang, X., Han, C., He, L., Wei, X., Niu, C., Zhao, K., Tian, X., Wei, Q., et al. (2016). Single-nanowire electrochemical probe detection for internally optimized mechanism of porous graphene in electrochemical devices. Nano Lett. *16*, 1523–1529.

115. Choi, C.S., Lau, J., Hur, J., Smith, L., Wang, C., and Dunn, B. (2018). Synthesis and properties of a photopatternable lithium-ion conducting solid electrolyte. Adv. Mater. *30*, 1703772.

116. Zhang, W., Weber, D.A., Weigand, H., Arlt, T., Manke, I., Schroder, D., Koerver, R., Leichtweiss, T., Hartmann, P., Zeier, W.G., et al. (2017). Interfacial processes and influence of composite cathode microstructure controlling the performance of all-solid-state lithium batteries. ACS Appl. Mater. Interfaces *9*, 17835–17845.

117. Khajehbashi, S.M.B., Xu, L., Zhang, G., Tan, S., Zhao, Y., Wang, L.S., Li, J., Luo, W., Peng, D.L., and Mai, L. (2018). High-performance Na-O_2 batteries enabled by oriented NaO_2 nanowires as discharge products. Nano Lett. *18*, 3934–3942.

118. Yue, J., Yan, M., Yin, Y.-X., and Guo, Y.-G. (2018). Progress of the interface design in all-solid-state Li–S batteries. Adv. Funct. Mater. https://doi.org/10.1002/adfm.201707533.

119. Xu, L., Zhao, Y., Owusu, K.A., Zhuang, Z., Liu, Q., Wang, Z., Li, Z., and Mai, L. (2018). Recent advances in nanowire-biosystem interfaces: from chemical conversion, energy production to electrophysiology. Chem *4*, 1538–1559.